Mechanism of Direct Electrophilic Aromatic Amination: an Electrophile is Found by Quantum-Chemical Study

Journal:	*The Journal of Organic Chemistry*
Manuscript ID	jo-2018-02814t
Manuscript Type:	Article
Date Submitted by the Author:	02-Nov-2018
Complete List of Authors:	Stankevich, Ksenia; National Research Tomsk Polytechnic University, Department of Biotechnology and Organic Chemistry Bondarev , Alexander; Altai State University, Department of Biomedicine Lavrinenko, Anastasia; National Research Tomsk Polytechnic University, The Kizhner Research Center Filimonov, Victor; Nacional'nyj issledovatel'skij Tomskij politehniceskij universitet, Department of Biotechnology and Organic Chemistry

SCHOLARONE™
Manuscripts

Mechanism of Direct Electrophilic Aromatic Amination: an Electrophile is Found by Quantum-Chemical Study

Ksenia S. Stankevich [a], Alexander A. Bondarev [b], Anastasia K. Lavrinenko [a],

Victor D. Filimonov [a],*

[a] The Kizhner Research Center, School of Advanced Manufacturing Technologies, National Research Tomsk Polytechnic University, Tomsk, 634050 Russia

[b] Department of Biomedicine, Altai State University, Barnaul, 656049 Russia

* corresponding author, filimonov@tpu.ru

Abstract

Direct amination is an extremely valuable reaction, allowing for the one-step preparation of aromatic amines. However, its' mechanism was poorly studied. Here, for the first time, using quantum chemical calculations, we have shown that direct amination of arenes by hydrazoic acid follows the classical S_EAr mechanism with aminodiazonium cation $H_2N_3^+$ (as) as electrophile. The $H_2N_3^+$ (as) has been found to be a very special diazonium cation with high dediazotization energy. The peculiarity of its electronic structure has been described using our novel method for tracing the molecular orbitals (MTMOs). The located stationary points and transition states allowed us to define direct amination as S_EAr reaction, which rate is determined by early transition state between π- and σ-complexes. Considering the calculated reaction constant ρ and an early transition state we placed direct amination of arenes by HN_3 somewhere in-between nitration and halogenations. Additionally, for the first time we have studied the acidity of hydrazoic acid and $H_2N_3^+$ and calculated their pK_a. We have shown that an acid stronger than $H_2N_3^+$ (as) with pK_a lower than approximately -5.32 is required for the direct amination with HN_3, justifying the use of superacids or Lewis acids. Our results explain the accumulated experimental data and open a prospect for the development of the new aminating agents working in milder conditions.

Keywords: direct amination, density functional theory, tracing the molecular orbitals, acidity, hydrazoic acid

Introduction

Aromatic amines are highly valuable building blocks in fine and industrial organic synthesis. Many biologically active compounds, dyes, agrochemicals, and polymers bear aromatic amino moieties [1]. Usually, anilines as well as heteroaromatic amines are prepared via nitration of the corresponding substrate, followed by the reduction of nitro group [2,3] or by other two- or multistep routes [4–8]. Considering an extremely high practical importance of aromatic amines, numerous attempts have been done to directly introduce amino group into aromatics via one-step route. For that purpose such nitrogen-containing compounds as ammonia [9,10], hydroxylamine, its salts and derivatives [11–13], and hydrazoic acid [14–19] were used. However, ammonia and hydroxylamines showed low aminating ability. For instance, in recent studies the yield of aniline from benzene using ammonia generated from ammonium carbonate was 10% at 300 °C and 300 bar in the presence of Rh/Ni-Mn/K-TiO$_2$ [10]. Amination of toluene by hydroxylammonium salts yielded in at most 65% of aminotoluidines using (NH$_2$OH)$_2$·H$_2$SO$_4$/AlCl$_3$ [11]. The amination of arenes with organic and inorganic azides in the presence of very strong protic or Lewis acids gave slightly better results [14–17]. In these conditions generated hydrazoic acid (HN$_3$) acts as the actual aminating agent. However, in this case satisfactory yields can be achieved with a limited number of aromatic substrates such as benzene and its derivatives with moderate electron-donating (e.g., alkylbenzenes) and electron-withdrawing (e.g., chlorobenzene) substituents. Nitrobenzene does not undergo amination by hydrazoic acid with practically significant yields [15]. Among benzenes with strong electron-donating substituents amination was reported for anisole [14,15], whereas no data is available for aniline. Only a few examples of successful direct amination of heterocyclic arenes are known. In instance, the amination of tetrazoles with hydroxylamine-O-sulfonic acid in weakly alkaline aqueous solutions resulted in a mixture of 1- and 2-N-aminotetrazoles in total yield of 38% [20]. N-alkylcarbazoles were aminated in 3,6-positions by NaN$_3$ in H$_2$SO$_4$ (yields are not given) [21]. Perimidine reacted with NaN$_3$ in polyphosphoric acid at 80-90 °C giving 6(7)-aminoperimidines in 62-76% yield [22]. Thus, unfortunately there is no general method of direct amination of arenes to date. First, it is due to fact that the described amination approaches use strong acidic and superacidic conditions, which are inapplicable to the majority of the desired substrates. The other reason for such unimpressive practical results in direct amination of aromatics is a lack of understanding of the possible reaction mechanisms. Unlike most other important electrophilic substitution reactions direct amination began to be studied much later. Therefore, not only have not been understood the details of the mechanism of this reaction, but even there is no unity in determining possible principal routes of aromatic amination. The understanding of mechanism of direct amination with hydrazoic acid and its derivatives is crucial to broaden the range of suitable

substrates and increase preparative yields. Thus, the aim of the study is to investigate possible pathways of electrophilic aromatic amination in nonpolar and polar media using quantum chemical calculations and identify the opportunities and limitations.

Overall, there are only several hypotheses regarding the mechanism of direct amination of arenes. According to the current knowledge, direct amination with HN_3 refers to electrophilic aromatic substitution reactions. It starts with the protonation of hydrazoic acid by a stronger acid giving aminodiazonium ion **1** [16] (Scheme 1). Considering previous studies, this step can be then followed by two different pathways. In the first one, the aminodiazonium cation **1** ($H_2N_3^+$ (□)) acts as an electrophile itself (pathway **A**), whereas in the second one it decomposes to nitrenium ion **2** (NH_2^+) and nitrogen (pathway **B**) (Scheme 1) [14–16,23]. In the latter case, the highly reactive nitrenium ion **2** acts as an electrophile. The available experimental results [14–16,23] do not allow to distinguish between the pathways **A** and **B**, thus both directions remain equally possible.

The completely different mechanism (pathway **C**) was proposed by Aksenov et al., who aminated arenes and pyrimidine using NaN_3 in the presence of polyphosphoric acid (PPA) [18]. The authors proposed the formation of PPA azide **3**, which is further protonated giving two tautomeric cations **4** and **5** (Scheme 1). The latest undergo azocoupling with arene and form intermediate triazenes **6** and **7**, which are then hydrolyzed giving the aromatic amine **8** (Scheme 1).
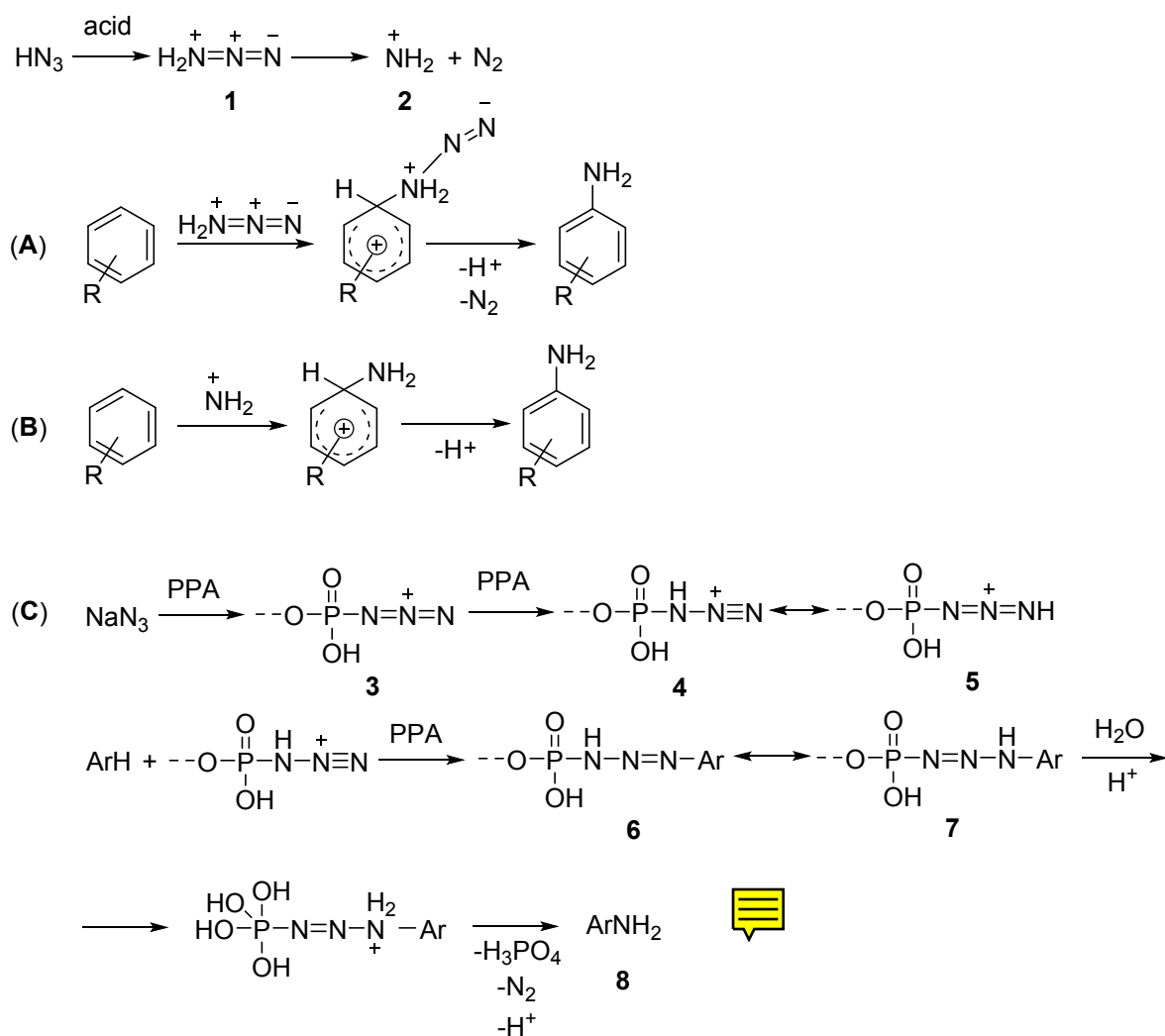
Scheme 1. Proposed mechanisms of direct electrophilic amination of arenes

Computational Methods

All the calculations were performed in Gaussian 09 (Revision-D.01-SMP) [24] and ORCA 3.0.2 [25] software.

Quantum Chemical Calculations

The structures of neutral molecules, ions, sigma complexes and transition states were fully optimized with Kohn−Sham density functional theory (DFT) using global-hybrid GGA functional B3LYP [26,27], range-separated hybrid meta-GGA functional M11 [28] or Møller–Plesset second-order perturbation theory (MP2) [29] and aug-cc-pVDZ [30,31] or 6-311++G(2df,2p) [32] basis sets. In each case the use of particular method is indicated. The stationary points were confirmed by harmonic frequency calculations. The transition states were characterized by imaginary vibrational mode and verified by intrinsic reaction coordinate calculation. The neutral molecules, ions, sigma

complexes and transition states were solvated using conductor-like polarizable continuum model (CPCM) or cluster-continuum model [33,34].

Method for tracing the molecular orbitals (MTMOs)

The energy dynamics and spatial distribution of the individual molecular orbitals (MOs) during the decomposition of singlet $H_2N_3^+$ (as) **1** were studied by relaxed potential energy surface (PES) scan by increasing the N_α-N_β distance (Fig.1) from 0.900 Å to 20 Å with a high resolution of 800 steps. The calculations were performed by DFT at B3LYP/aug-cc-pVDZ level of theory using ORCA 3.0.2 software. According to the data obtained, the dependences of the energies of all MOs on the N_α-N_β distance during the process of spatial separation of NH_2^+ and N_2 were found. The number of orbitals in the initial molecular system ($H_2N_3^+$ (as)) exactly corresponded to the total number of orbitals of the fragments formed (NH_2^+ and N_2). By revealing the correspondence between the MOs of the $H_2N_3^+$ (as) and the MOs of the decomposition products (NH_2^+ and N_2), the energy diagram of the MOs transition was constructed. Then, the contribution of each MO and the total contribution of each fragment to the formation of the $H_2N_3^+$ (as) were calculated. To perform the tracing, comparing and visualizing of the spatial distribution of the electronic density, the special software was developed and applied [35].

Calculation of pK_a

By definition, the pK_a of hydrazoic acid can be quantified using the following proton-transfer reaction (eq 1):

$$HN_3 + H_2O \rightarrow N_3^- + H_3O^+ \tag{1}$$
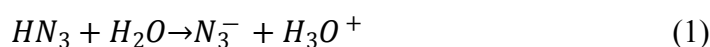
However, it is known that the formation of charged species from neural molecules is a challenging task for theoretical calculations. To conserve the number of charged species we chosen eq 2 instead of 1 as it was done in [33]:

$$HN_3 + OH^- \rightarrow N_3^- + H_2O \qquad \Delta G_{sol}^* \tag{2}$$

The pK_a of hydrazoic acid was then calculated using the following expression [33]:

$$pK_a(HN_3) = \frac{\Delta G_{sol}^*}{(2.303)RT} + 15.74 \tag{3}$$

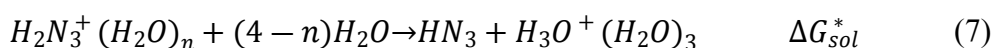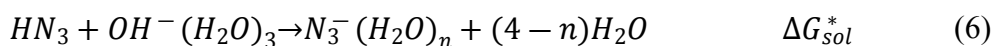The reaction shown in eq 4 was used for the pK_a calculation of $H_2N_3^+$,

$$H_2N_3^+ + H_2O \rightarrow HN_3 + H_3O^+ \qquad \Delta G_{sol}^* \tag{4}$$
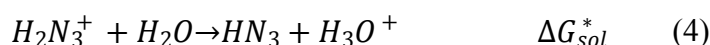
with the pK_a calculated according to the eq 5 [33]:

$$pK_a\left(H_2N_3^+\right) = \frac{\Delta G_{sol}^*}{(2.303)RT} - 1.74 \qquad (5)$$

We found the solvation free energy (ΔG_{sol}*) of hydrazoic acid and $H_2N_3^+$ using two different solvation models: conductor-like polarizable continuum model (CPCM) and cluster-continuum model [33,34].

In CPCM the pK_a was found using the data generated by calculations at B3LYP/aug-cc-pVDZ level of theory and eqs 3 and 5. Whereas in cluster-continuum model the calculations were performed as described below.

The cluster-continuum model implies that the ion is represented as a cluster formed by the ion and an optimal number of solvent molecules that is then solvated using a dielectric continuum [33,34]. For example, for the OH$^-$ and H_3O^+ ions the optimum number of water molecules was shown to be three [34]. Thus, in the cluster-continuum model the following reactions 6 and 7 would describe the ionization of hydrazoic acid and $H_2N_3^+$, respectively [33]:

$$HN_3 + OH^-(H_2O)_3 \rightarrow N_3^-(H_2O)_n + (4-n)H_2O \qquad \Delta G_{sol}^* \qquad (6)$$

$$H_2N_3^+(H_2O)_n + (4-n)H_2O \rightarrow HN_3 + H_3O^+(H_2O)_3 \qquad \Delta G_{sol}^* \qquad (7)$$

The pK_a of hydrazoic acid and $H_2N_3^+$ can be then calculated using eqs 8 and 9 [33]:

$$pK_a(HN_3) = \frac{\Delta G_{sol}^*}{(2.303)RT} + 15.74 + (3-n)\log[H_2O] \qquad (8)$$

$$pK_a\left(H_2N_3^+\right) = \frac{\Delta G_{sol}^*}{(2.303)RT} - (4-n)\log[H_2O] \qquad (9)$$

Using a variational principle, we have found that the optimum number of water molecules for the azide anion N_3^- equals two, whereas for $H_2N_3^+$ (both symmetrical and asymmetrical) it was either two or three depending on calculation method. We obtained the structures of ionic clusters and neutral species by optimization at the MP2/6-311++G(2df,2p) and M11/6-311++G(2df,2p)//B3LYP/6-311++G(2df,2p) level of theory. In the second case, after performing a frequency job using M11/6-311++G(2df,2p) we took the full electronic energy of the system and added the correction to Gibbs free energy from B3LYP/6-311++G(2df,2p) calculation. The solvation free energy (ΔG_{sol}*) of clusters and neutral molecules by the bulk solvent (water) was calculated by CPCM.

Calculation of rate constants

The reaction rate constants were calculated using Eyring–Polanyi eq 10:

$$k = \frac{\kappa k_B T}{h} \cdot e^{\frac{-\Delta G^{\neq}}{RT}} \qquad (10)$$

where $\Delta G^{\neq}$ is the Gibbs energy of activation, κ is the transmission coefficient ($\kappa = 1$), k_B is Boltzmann's constant, h is Planck's constant, R is gas constant, and T is absolute temperature ($T = 298.15$ K).

Results and discussion

Structure of hydrazoic acid and related compounds

Since the molecular geometry of hydrazoic acid is well described experimentally [36], we used it for the justification of the chosen B3LYP/aug-cc-pVDZ level of theory. The calculated and experimental values of bond distances (angstroms) and bond angles (degrees) of HN_3 are summarized in Table 1.

Table 1. Calculated and experimentally determined geometries of HN_3, $H_2N_3^+$ (as) (singlet, Fig. 1) and NH_2^+.

	HN_3		$H_2N_3^+$ (as)				NH_2^+ (singlet)		NH_2^+ (triplet)	
	expt[a]	calc[d]	expt[b]	calc[d]	3-21G[b]	LDF[b]	MP4[c]	calc[d]	MP4[c]	calc[d]
	Bond distances, Å									
N_α-N_β	1.233	1.245	1.295	1.288	1.305	1.276	-	-	-	-
N_β-N_γ	1.121	1.138	1.101	1.116	1.088	1.126	-	-	-	-
N_α-H	≈1.02	1.023	-	1.024	1.008	1.043	1.043	1.061	1.025	1.043
	Bond angles, deg									
N_α-N_β-N_γ	172.8	171.1	175.3	175.7	na	175.2	-	-	-	-
H-N_α-N_β	109	109.9	107.6	115.2	na	114.5	-	-	-	-
H-N_α-H	-	-	118.8	121.08	na	117.9	107.1	106.9	149.4	154.1

[a] Data from ref. [36]; [b] Data from ref. [37]; [c] Data from ref. [38], calculations performed at MP4/6-311+G(3d,2p); [d] according to our results obtained using B3LYP/aug-cc-pVDZ; na - data not available

The lowest energy structure found for hydrazoic acid using B3LYP/aug-cc-pVDZ is in good agreement with experimentally determined one [36] (Table 1). However, absorption bands assigned to in and out of plane bending of N-N-N moiety in calculated infrared (IR) spectrum of hydrazoic acid are shifted in comparison to experimental values (Table 2). It could be caused by the differences in predicted and observed values of N_α-N_β-N_γ angle - 172.8° and 171.1°, respectively.

Table 2. Calculated and observed IR absorption bands of HN_3 and $H_2N_3^+$ (as).

	Frequency, cm^{-1}			Frequency, cm^{-1}		
Assignment	HN_3		Assignment	$H_2N_3^+$ (as)		
	expt[a]	calc[b]		expt[c]	calc[c]	calc[b]

ν N-H	3336	3372	ν_{as} NH$_2$	3280	3372	3447
ν N$_\beta$-N$_\gamma$	2140	2199	ν_{sym} NH$_2$	3170	3248	3313
δ_{sciss} NH	1269	1258	ν N≡N	2318	2350	2325
δ NH against linear group	1152	1152	δ_{sciss} NH$_2$	1547	1526	1537
δ N-N-N out of plane	739	573	δ_{as} NH$_2$	1259	1232	1227
δ N-N-N in plane	658	511	ν N-N	1129	1190	1134
			δ N-N-N in plane	530	516	501
			δ_{wag} NH$_2$	489	479	319
			δ N-N-N out of plane	418	429	376

[a] Data from ref. [36]; [b] according to our results obtained using B3LYP/aug-cc-pVDZ level of theory (scale factor 0.97); [c] Data from ref. [37];

The protonated hydrazoic acid ($H_2N_3^+$), that is supposed to play one of the key roles in direct amination reaction, could have symmetric ($H_2N_3^+{}_{(s)}$) or asymmetric **1** ($H_2N_3^+{}_{(as)}$) structure (Fig.1). To find the lowest energy structure for both of them, we scanned the potential energy surface varying the H-N-N-N dihedral and N-N-N bond angles. The predicted $H_2N_3^+{}_{(s)}$ structure had C_2 symmetry, N-N-N angle of 166.8° and N-N bond distance of 1.18 Å. Whereas $H_2N_3^+{}_{(as)}$ structure **1** had C_s symmetry with a pyramidal amino group (Fig.1), N-N-N angle of 175.7° and NH$_2$-N bond distance of 1.288 Å. This is in agreement with experimental data and previous calculations by LDF theory [37] (Table 1). On the other hand, the calculations showed NH$_2$-N moiety flatter than it appears, resulting in less accurate predictions of the frequency of vibrations associated with its stretching and bending (Table 2). The **1** $H_2N_3^+{}_{(as)}$ has an increased N$_\alpha$-N$_\beta$ distance and decreased N$_\beta$-N$_\gamma$ distance as compared to hydrazoic acid indicating its' structural similarity with the RN$_2^+$ diazonium cations [39]. Our calculations show that **1** $H_2N_3^+{}_{(as)}$ is favored by 25.18 kcal/mol over $H_2N_3^+{}_{(s)}$. This is in agreement with the results of previous calculations at 3-31G level of theory, where energy difference was found to be 49.8 kcal/mol. The studies of the crystal structure of **1** $H_2N_3^+$ salts also proved that $H_2N_3^+$ cation has asymmetric aminodiazonium structure [37].

Recall, that there are two options for aminodiazonium cation in amination reaction: it could attack aromatic ring itself (pathway **A**, Scheme 1) or decompose to highly reactive nitrenium ion (pathway **B**, Scheme 1). It is known that nitrenium ion can exist in either singlet or triplet state [38]

and among them the triplet state is more favorable one. Considering that direct amination involves the formation of nitrenium ion from aminodiazonium cation, we assumed that $H_2N_3^+$ could also exist in singlet and triplet state. According to the results triplet states for both $H_2N_3^+$ $_{(s)}$ and $H_2N_3^+$ $_{(as)}$ are much less favourable then singlet states (Fig.1). It is interesting that the energy difference between $H_2N_3^+$ $_{(as)}$ and $H_2N_3^+$ $_{(s)}$ in triplet state is only 3.88 kcal/mol. Both of them were predicted to be flat with significantly decreased N-N-N angle (Fig.1). For $H_2N_3^+$ $_{(as)}$ in triplet state structure having C_2 symmetry, N-N-N angle of 117.9° and N-N bond distance of 1.18 Å was found, whereas for $H_2N_3^+$ $_{(s)}$ in triplet state structure having C_{2V} symmetry, N-N-N angle of 126.6° and N-N bond distance of 1.27 Å was found.

The study of nitrenium ion geometry in singlet and triplet state using B3LYP/aug-cc-pVDZ level of theory predicted values of bond distances and angles close to ones calculated previously at (MP4/6-311+G(3d,2p)) [38] (Table 1), except the H-N-H angle in triplet, which is noticeably higher. The triplet state was favored by 33.14 kcal/mol over singlet state, which is in agreement with experimental value of 30.09 kcal/mol [40].

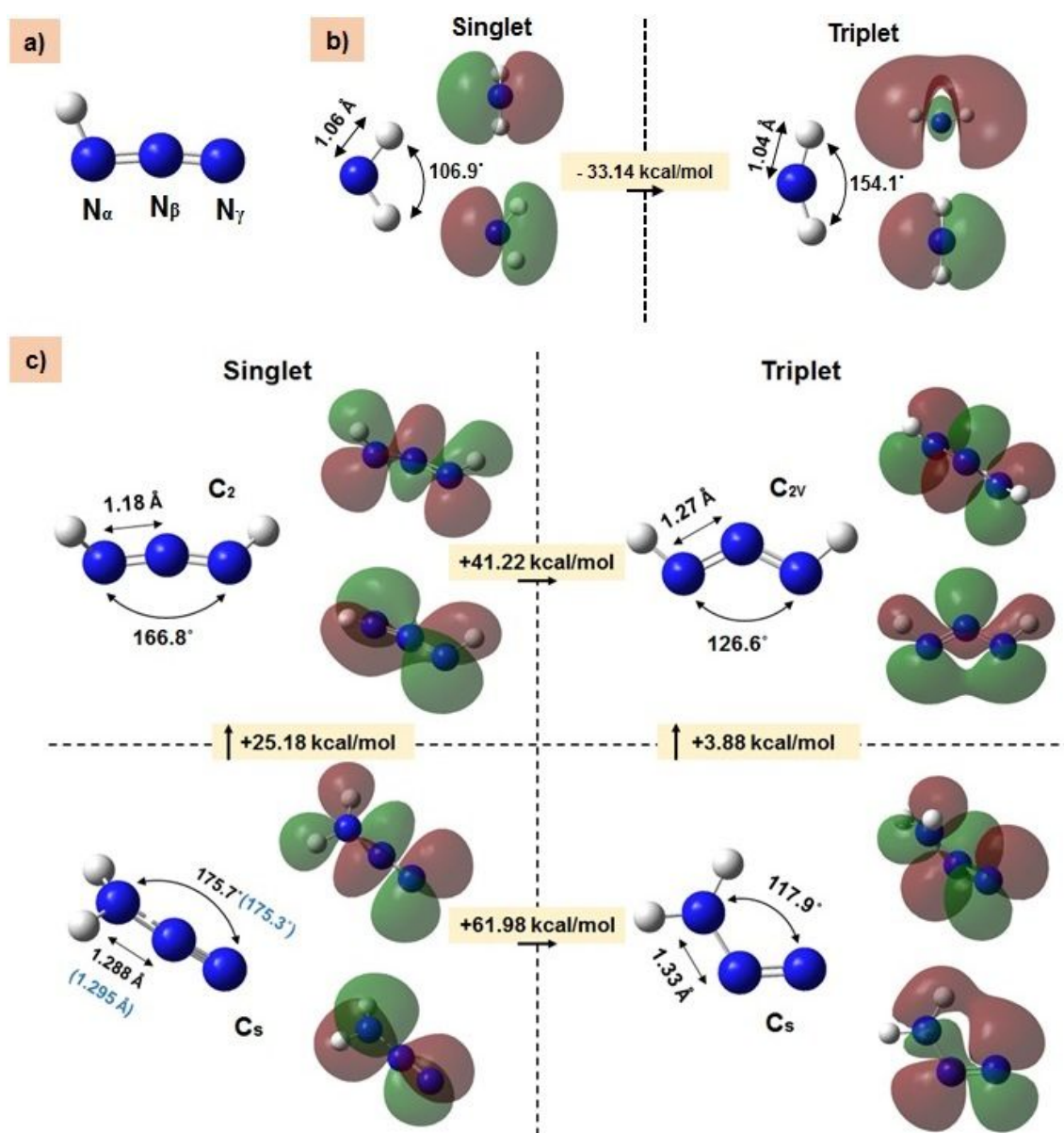Thus, the chosen level of theory proved to be appropriate and was used for further calculations.

Fig.1 Structure of hydrazoic acid (a) and geometries and MO representation (LUMO above HOMO) of intermediates generated from it: b) NH_2^+ in singlet and triplet state and c) $H_2N_3^+{}_{(as)}$ and $H_2N_3^+{}_{(s)}$ in singlet and triplet state. The bond distances (angstroms) and bond angles (degrees) are shown according to the results of calculations at B3LYP/aug-cc-pvdz level of theory. For $H_2N_3^+{}_{(as)}$ experimental values are shown in blue.

Acidity of hydrazoic acid, $H_2N_3^+{}_{(as)}$ and $H_2N_3^+{}_{(s)}$

Regardless of whether the direct amination proceeds with **1** $H_2N_3^+{}_{(as)}$ or **2** NH_2^+ as electrophile, the crucial step for these species' formation is a protonation of hydrazoic acid (Scheme 1). To identify the conditions, in which the protonation occurs, the pK_a values of hydrazoic acid and $H_2N_3^+$ are necessary. Here, for the first time we have studied the acidity of hydrazoic acid and $H_2N_3^+$ and calculated their pK_a using both continuum and cluster-continuum solvation models.

The pK_a calculated for hydrazoic acid using CPCM at B3LYP/aug-cc-pvdz showed poor agreement with experimental value and deviation approaching 10.6 pK_a units (eqs 2,3, Table 3) [41]. Such a result can be explained by the general drawbacks suffered by continuum solvation models. In particular, they do not consider strong and specific interaction between solvent molecules in first coordination shell and solute. Also, continuum behavior is not observed near the solute molecules [34]. Overall, it was shown that ions of organic molecules with the charge localized on nitrogen are poorly described by continuum solvation models [33,34]. In this case, the better performance was achieved by using cluster-continuum solvation model, where the ion is represented as a cluster formed by the ion and an optimal number of solvent molecules that is then solvated using a dielectric continuum. [33,34]. Following this method, we built clusters formed by the ion and an optimal number of solvent molecules for all the charged species and calculated pK_a values (eqs 6-9, Table 3). For the OH$^-$ and H$_3$O$^+$ ions the optimum number of water molecules was previously shown to be three [34]. Using a variational principle, we have found that the optimum number of water molecules for the azide anion N$_3^-$ equals two, whereas for H$_2$N$_3^+$ it was either two or three depending on calculation method.

Table 3. Predicted and experimental pK_a values of hydrazoic acid and H$_2$N$_3^+$ species.

Compound	Experimental	CPCM[a]	Cluster-continuum model[b]	Cluster-continuum model[c]
HN$_3$	4.92 [41]	-5.65	1.89	4.39
H$_2$N$_3^+$ $_{(as)}$	-	3.88	-7.85	-5.32
H$_2$N$_3^+$ $_{(s)}$	-	-10.91	-18.15	-17.45

[a] B3LYP/aug-cc-pvdz; [b] MP2/6-311++G(2df,2p) (N$_3^-$(H$_2$O)$_3$ cluster); [c] M11/6-311++G(2df,2p)//B3LYP/6-311++G(2df,2p) (N$_3^-$(H$_2$O)$_2$ cluster)

The cluster-continuum model at MP2/6-311++G(2df,2p) predicted pK_a of 1.89 for hydrazoic acid. This is much closer to experimental value than pK_a obtained by CPCM. The pK_a values for H$_2$N$_3^+$ $_{(as)}$ and H$_2$N$_3^+$ $_{(s)}$ were found to be -7.85 and -18.15, respectively.
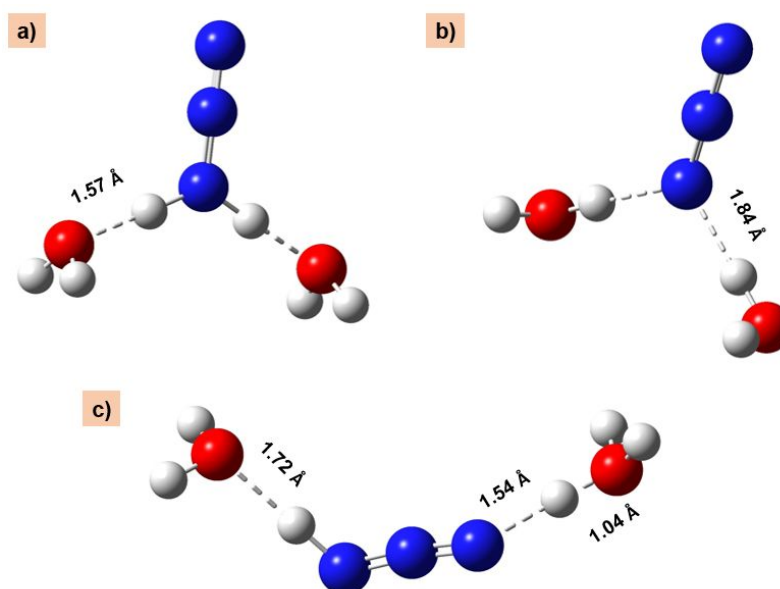
Fig. 2. Optimized geometries for the clusters (B3LYP/6-311++G(2df,2p)): a) $H_2N_3^+$ (as) $(H_2O)_2$; b) N_3^- $(H_2O)_2$; c) $H_2N_3^+$ (s) $(H_2O)_2$.

In order to improve the accuracy pK_a calculations we conducted geometry optimization of the obtained clusters using B3LYP functional, which has already shown good results for geometry prediction of the studied species (Table 2). Then, we performed a frequency job with Gaussian09 using range-separated hybrid meta-GGA functional M11 intended for main group thermochemistry [28] the calculated pK_a for hydrazoic acid was 4.39, much less deviating from the experimental value than pK_a found at MP2/6-311++G(2df,2p) level of theory. The pK_a values for $H_2N_3^+$ (as) and $H_2N_3^+$ (s) were found to be -5.32 and -17.45, respectively.

The geometries of the obtained clusters are shown in Fig. 2. The $H_2N_3^+$ (as) is strongly solvated: the hydrogen bond distance in $H_2N_3^+$ (as) $(H_2O)_2$ is close to the one in $H_3O^+(H_2O)_3$ (Fig.1S a, Supporting) and is shorter than in N_3^- $(H_2O)_2$ (Fig.2b). The $H_2N_3^+$ (s) $(H_2O)_2$ geometry shows the proton transfer from $H_2N_3^+$ (s) to H_2O (Fig.2a).

Thus, the $H_2N_3^+$ (s) and $H_2N_3^+$ (as) were predicted to be much stronger acids then HN_3. In turn, the $H_2N_3^+$ (s) was predicted to be a stronger acid than $H_2N_3^+$ (as). This is in agreement with the fact that $H_2N_3^+$(as) is more thermodynamically favourable and, therefore, more stable than $H_2N_3^+$(s). Considering previous studies of $H_2N_3^+$ structure [16,37], it is unlikely that the $H_2N_3^+$ (s) can be obtained experimentally or participates in direct amination. Therefore, its' pK_a calculation has rather academic interest than practical. In contrast, the pK_a found for **1** $H_2N_3^+$ (as) has a great practical importance since it allows us not only to explain the accumulated experimental results, but also to finally clarify the conditions required for direct amination. It was observed that direct amination using N_3^- does not proceed in trifluoroacetic acid [14] (pK_a = 0.52 [42]) and gives poor yields in sulfuric acid [17] ($pK_a(1)$ = -2.8; $pK_a(2)$ = 1.92), whereas better results were obtained using CF_3SO_3H (H_0 =

-14.1[15]) [14,23], CF_3COOH/CF_3SO_3H [14], BF_3-H_2O (H_0 = -11.4) [15], $AlCl_3$-HCl [16,43] (H_0 = -0.92) and $AlCl_3$-H_2SO_4 [44]. Considering predicted pK_a for $H_2N_3^+$ (as) we can conclude that CF_3COOH and H_2SO_4 are stronger than hydrazoic acid but weaker than $H_2N_3^+$ (as) (Table 3), while in other cases acids are stronger then both hydrazoic acid and $H_2N_3^+$ (as) (Table 3). Thus, an acid stronger than $H_2N_3^+$ (as) with pK_a lower than approximately -5.32 is required for the direct amination with HN_3. As we can see, such an acid can be found among superacids or Lewis acids.

Mechanism of direct amination

Herein, we consider two possible pathways **A** and **B** of direct amination (Scheme 1) proposed earlier elsewhere [14–16,23]. Both of them refer to electrophilic aromatic substitution. However, in the first one the **1** $H_2N_3^+$ (as) acts as electrophile (pathway **A**), while in the second one the **1** $H_2N_3^+$ (as) decomposes giving **2** NH_2^+, which then acts as electrophile (pathway **B**) (Scheme 1).

If we assume that direct amination follows the pathway **B** we need to assess the energy required for the NH_2^+ generation.
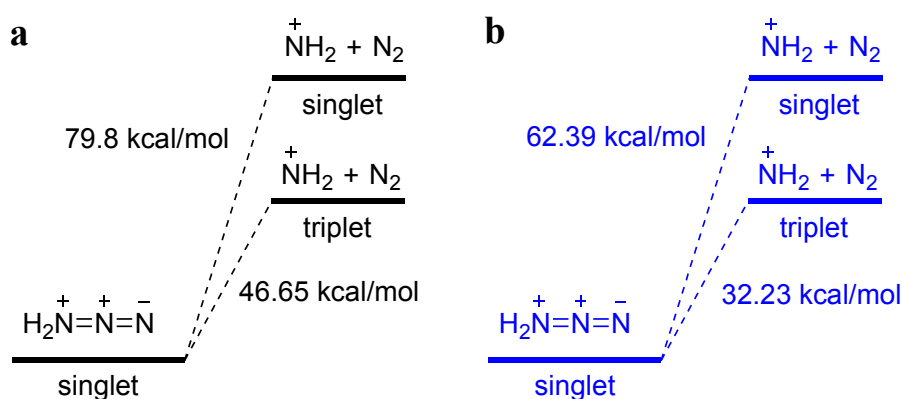

Scheme 2. Thermodynamic characteristics of NH_2^+ formation from $H_2N_3^+$ (as) calculated at B3LYP/aug-cc-pvdz level of theory in (a) gas phase and (b) water (CPCM solvation model).

As can be seen from Scheme 2 (a), the energy of bare **2** NH_2^+ formation from **1** $H_2N_3^+$ (as) is 79.8 kcal/mol. This energy difference can be reduced to 46.65 kcal/mol if NH_2^+ appears in triplet state. However, nitrenium ion in singlet state has a vacant *p* orbital and a lone electron pair, thus, it is more likely that it would act as electrophile. Thus, in pathway **B** the energy required for the generation of electrophile is 79.8 kcal/mol. Solvation decreases the energy of NH_2^+ formation from $H_2N_3^+$ (as) to 62.39 kcal/mol (Scheme 2 (b)). It is important to note that the energy of N_α-N_β bond cleavage in $H_2N_3^+$ (as) is significantly higher than the energy of nitrogen elimination from aromatic

diazonium cation PhN_2^+ (eq 11). The latter equals 30 kcal/mol according to experimental data and theoretical calculations [see, for example, [45]].

$$PhN_2^+ \rightarrow Ph^+ + N_2 \qquad (11)$$
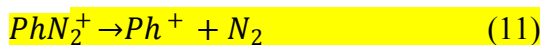
Such a high strength of N_α-N_β bond in **1** $H_2N_3^+$ (as) is due to a high free energy of NH_2^+ (singlet) comparing to Ph^+. Thus, if we consider only dediazotization energy as a criterion of diazonium cations stability, we can conclude that among aryl- and alkyl-diazonium cations aminodiazonium cation $H_2N_3^+$ (as) should be the most stable one.

For a deeper understanding of N_α-N_β bond nature in **1** $H_2N_3^+$ (as) we used a method for tracing the molecular orbitals (MTMOs), developed by us [35]. MTMOs allows revealing the correspondence between the MOs of the $H_2N_3^+$ (as) and the MOs of the decomposition products (NH_2^+ and N_2), therefore giving an understanding, which MO of the decomposition products participates in the $H_2N_3^+$ (as) MO formation.

The energies of individual MO over increasing N_α-N_β distance during N_2 elimination from $H_2N_3^+$ (as) in the area close to LUMO and HOMO are shown in Fig. 2S (Supporting). The energy diagram of the formation of **1** $H_2N_3^+$ (as) from **2** NH_2^+ and N_2 is presented in Fig. 3S (Supporting). Considering the spatial similarity of MOs, it was found that $H_2N_3^+$ (as) occupied MOs 1, 3, 4, 6, 9, 10, and 11 appear as a result of transformation of occupied MOs of N_2, whereas $H_2N_3^+$ (as) occupied MOs 2, 5 7, 8 are formed by occupied MOs of NH_2^+ (Table 4).

Among the unoccupied MOs of $H_2N_3^+$ (as) that are also appear as a result of transformation of MOs of decomposition products, the most interesting are 12, derived from N_2, and 13 and 14, derived from NH_2^+ (Table 4). The $H_2N_3^+$ (as) occupied MO 11 is formed during the transformation of N_2 HOMO, while $H_2N_3^+$ (as) unoccupied MO 14 appear as a result of the transformation of NH_2^+ LUMO. The peculiarity of the $H_2N_3^+$ (as) formation is that the N_2 HOMO energy (-0.438559 Ha) is higher than the NH_2^+ LUMO energy (-0.610093 Ha). This causes a very strong interaction between these orbitals. The high interaction energy leads to a very slow separation of the orbitals during an increase in N_α-N_β distance. This process continues up to a distance of 50 Å. At short distances there is only a tendency towards separation. Fig.3 shows this very special case where at N_α-N_β distance of 11.91 Å MO11 of $H_2N_3^+$ (as) only tends to localize on N_2 and spatially corresponds to MO 7 of N_2 (HOMO), whereas MO 14 of $H_2N_3^+$ (as) tends to transform into the MO 6 (LUMO) of the NH_2^+. All other MOs are already localized on N_2 or NH_2^+ at distances of less than 6 Å. The videos of all MO transformations are given in Supporting.

We also considered different charge distribution between $H_2N_3^+$ (as) decomposition products, e.g. N_2^+ and NH_2. However, the analysis of structural parameters (Table 1S, Supporting) shows that at high distances, the system tends to the state close to free species NH_2^+ and N_2. Thermodynamics

analysis (Table 2S, Supporting) also confirms that the formation of N_2^+ and NH_2 is much less favorable (ΔG^{298}=144.3 kcal/mol) than the formation of NH_2^+ and N_2 (ΔG^{298}=74.2 kcal/mol).
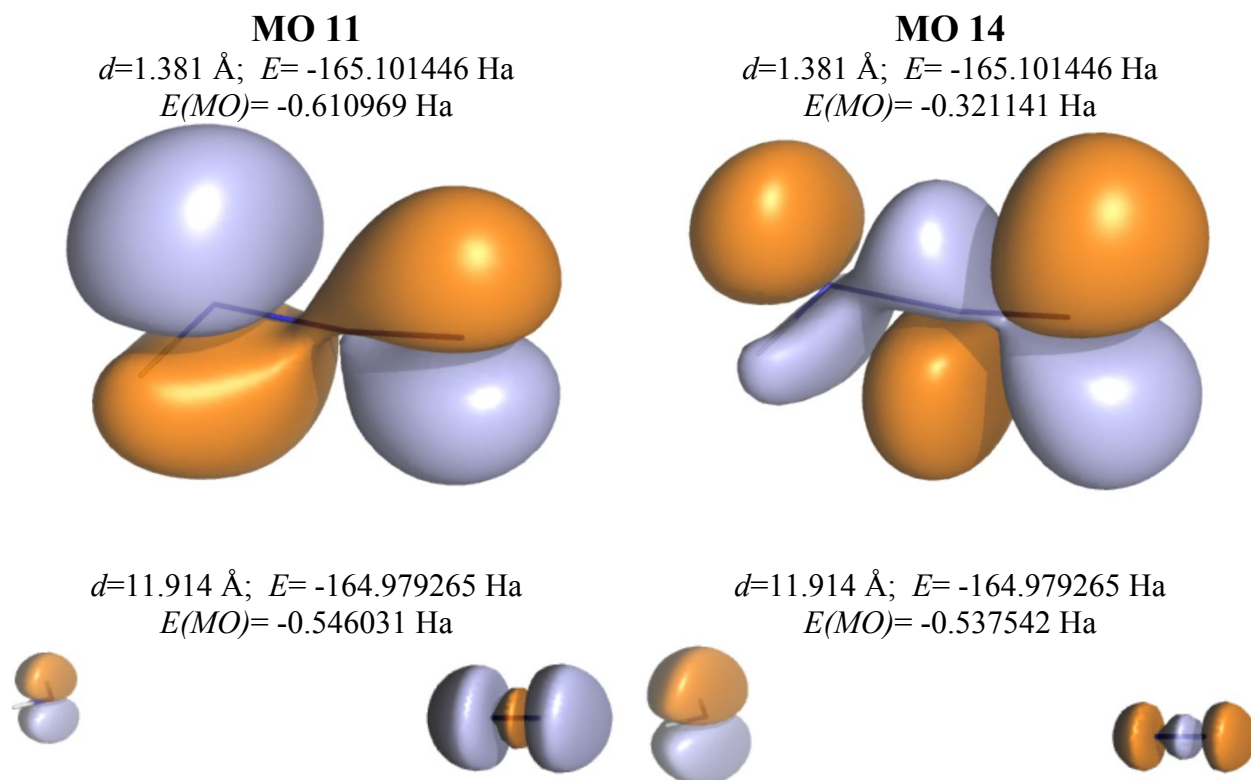

MO 11
d=1.381 Å; *E*= -165.101446 Ha
E(MO)= -0.610969 Ha

MO 14
d=1.381 Å; *E*= -165.101446 Ha
E(MO)= -0.321141 Ha

d=11.914 Å; *E*= -164.979265 Ha
E(MO)= -0.546031 Ha

d=11.914 Å; *E*= -164.979265 Ha
E(MO)= -0.537542 Ha

Fig. 3. A special case of $H_2N_3^+$ (as) 11 and 14 MOs transformation into N_2 MO and NH_2^+ MO, respectively. The MOs separation is very slow and continues up to a N_α-N_β distance of 50 Å.

The energy changes of each single MO during the formation of $H_2N_3^+$ (as) from NH_2^+ and N_2 are shown in Table 4.

Table 4. The energy changes of each MO during the formation of $H_2N_3^+$ (as) from NH_2^+ and N_2.

Occupied Molecular Orbitals							
MO, №	E_{MO} (N_2), Ha	E_{MO} (NH_2^+), Ha	E_{MO} ($NH_2N_2^+$), Ha	ΔE_{MO} (N_2), Ha	ΔE_{MO} (NH_2^+), Ha	ΔE_{MO}, Ha	ΔE_{MO}, %
1[a]	-14.450116		-14.813807	-0.363691		-0.363691	18.1
2[b]		-14.889393	-14.747831		0.141562	0.141562	-7.0
3	-14.44860		-14.719726	-0.271126		-0.271126	13.4
4	-1.134986		-1.458669	-0.323683		-0.323683	16.1
5		-1.265568	-1.298670		-0.033102	-0.033102	1.6
6	-0.565855		-0.965855	-0.400000		-0.400000	19.9
7		-0.891819	-0.886050		0.005769	0.005769	-0.3
8		-0.744735	-0.809290		-0.064555	-0.064555	3.2

9	-0.471908		-0.747709	-0.275801		-0.275801	13.3
10	-0.471925		-0.738254	-0.266329		-0.266329	13.2
11c	-0.438559		-0.600942	-0.162383		-0.162383	8.1
Σ, Ha	-31.981949	-17.791515	-51.786803	-2.063013	0.049674	-2.013339	
Σ, %	61.8	34.4		102.5	-2.5		
Unoccupied Molecular Orbitals							
MO, №	E_{MO} (N_2), Ha	E_{MO} (NH_2^+), Ha	E_{MO} ($NH_2N_2^+$), Ha	ΔE_{MO} (N_2), Ha	ΔE_{MO} (NH_2^+), Ha	ΔE_{MO}, Ha	ΔE_{MO}, %
12	-0.039746		-0.338540	-0.298794		-0.298794	
13		-0.265744	-0.199308		-0.033564	-0.033564	
14		-0.610093	-0.235372		0.374721	0.374721	

[a] MOs of $H_2N_3^+$ (as) derived from MOs of N_2 are shown in green; [b] MOs of $H_2N_3^+$ (as) derived from MOs of NH_2^+ are shown in yellow; [c] A special case of $H_2N_3^+$ (as) 11 and 14 MOs transformation into N_2 MO and NH_2^+ MO, respectively is shown in red.

Energy calculations showed that the main contribution to reducing the total energy of all occupied orbitals of $H_2N_3^+$ (as) is made by MOs derived from N_2 MOs transformation (Table 4). These MOs significantly reduce their energy (102.5% of the change in total MO energy). On the contrary, the $H_2N_3^+$ (as) orbitals formed as a result of the transformation of the NH_2^+ MOs change their energy slightly and in different directions, overall increasing the energy (-2.5%). It is interesting that all orbitals of N_2 reduce their energy to a comparable extent, including more deeply lying internal MOs.

Therefore, apparently, the main reason for the interaction between NH_2^+ and N_2 with a decrease in energy and the formation of a very strong chemical bond is the possibility of additional delocalization of electrons of the N_2 molecule on the nuclei of the nitrogen and hydrogen atoms of NH_2^+.

If we now consider pathway **A** for direct amination we need to locate the structures and free energies of stationary points on the potential energy surface (PES) of the reaction. Using benzene as an example, we followed the classical electrophilic aromatic substitution mechanism and found the structures and free energies of π-complex, σ-complex and corresponding transition states (Fig.4, Scheme 3).
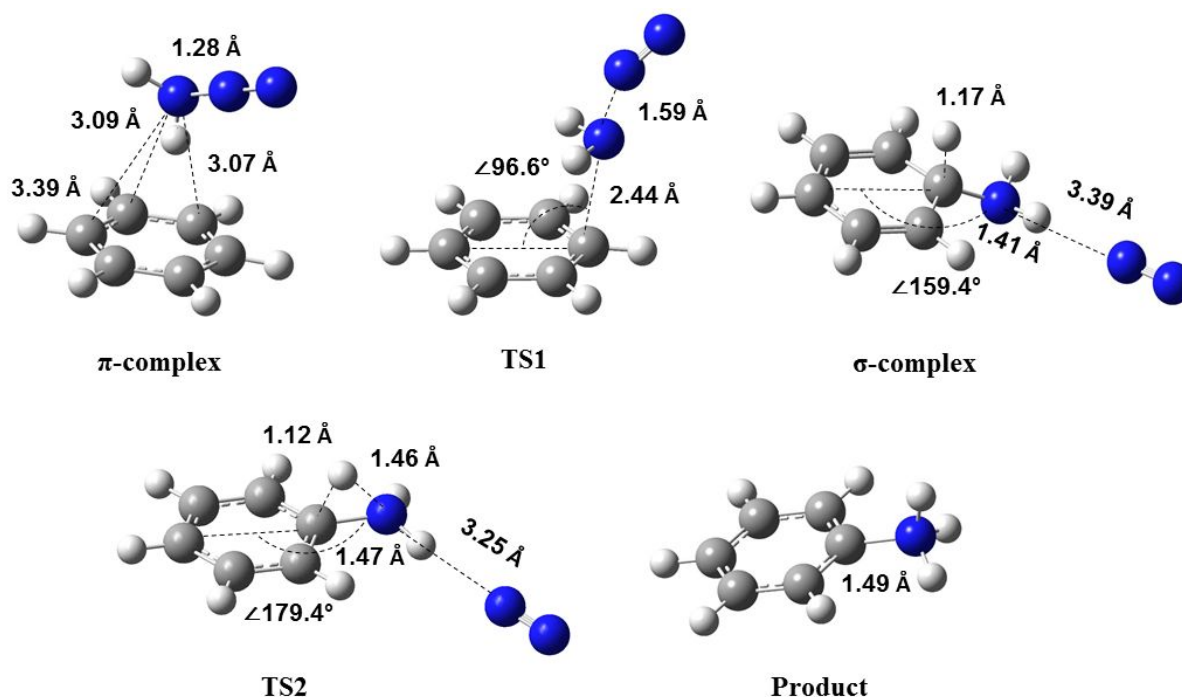
Fig.4. Structures of the stationary points on the potential energy surface in the direct amination of benzene by $H_2N_3^+{}_{(as)}$. The bond distances (angstroms) and bond angles (degrees) are shown according to the results of calculations at B3LYP/aug-cc-pvdz level of theory.

The calculation results predict amination to be thermodynamically favorable. The Gibbs free energy change in the reaction of anilinium ion and nitrogen formation from benzene and $H_2N_3^+{}_{(as)}$ is -85.75 kcal/mol (eq 12).

$$C_6H_6 + H_2N_3^+{}_{(as)} \rightarrow PhNH_3^+ + N_2 \qquad (12)$$
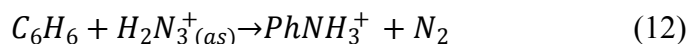
The data for the substituted arenes are given in Table 5 and will be discussed further. Here we should only note that amination remains thermodynamically favorable for both activated and deactivated substrates.

As can be seen from Fig.4, benzene and **1** $H_2N_3^+{}_{(as)}$ form a C atom coordinated π-complex with a C-N distances of 3.07-3.39 Å. The strong interaction and charge transfer between **1** $H_2N_3^+{}_{(as)}$ and benzene in π-complex facilitate the further decomposition of **1** $H_2N_3^+{}_{(as)}$ observed in TS1 (-523.52 cm^{-1}). The geometry of TS1 shows an increased N_α-N_β bond length of 1.59 Å in **1** $H_2N_3^+{}_{(as)}$ specie and decreased C_{Ar}-N_α distance of 2.44 Å indicating that N_α-N_β bond cleavage in **1** $H_2N_3^+{}_{(as)}$ is accompanied by simultaneous formation of C- N_α bond between appearing **2** NH_2^+ and benzene. In σ-complex the C-N_α distance reduces to 1.41 Å, whereas N_α-N_β distance increases to 3.39 Å demonstrating the final appearance of C-N_α bond and release of nitrogen. A comparison of the C-N distance in π-complex, TS1, and σ-complex shows that TS1 has a structure more similar to π-complex. Thus, according to the Hammond postulate the direct amination has an earlier transition state than halogenations since halogenations show a closer structural similarity between

the σ-complex and corresponding transition state [46–48]. Considering the structure of the σ-complex it seems likely that the amino group would serve as a base in the deprotonation of the arenium ion. Indeed, the found TS2 structure (-1441.53 cm^{-1}) shows the proton moving half-way towards amino group and increased C-N bond length of 1.47 Å close to one in anilinium ion (1.49 Å). The deprotonation of the arenium ion and release of nitrogen result in formation of the anilinium ion, which structure is shown in Fig.4.
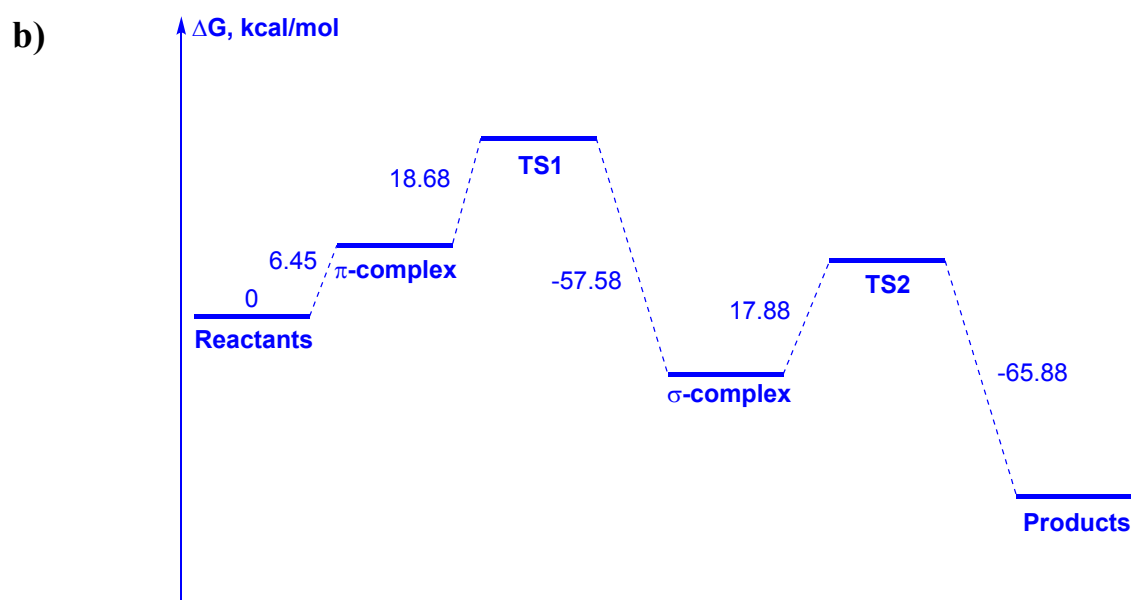
The PESs for the direct amination of benzene by **1** $H_2N_3^+$ $_{(as)}$ in gas phase and in water are shown in Scheme 3. The formation of the π-complex in gas phase is an exergonic process by -3.23 kcal/mol, whereas in aqueous solution it is endergonic by 6.45 kcal/mol. Thus, in water the reactants are better solvated than π-complex. The similar changes in energy were observed for the formation of the π-complex in aqueous and gas phase in nitration [46]. The rest of the PES profile is similar for the gas phase and water.

As we can see in both gas phase and water the rate determining step in benzene amination by **1** $H_2N_3^+$ $_{(as)}$ is the transition state TS1 between π- and σ-complexes, which formation from π-complex in gas phase requires 14.93 kcal/mol (Scheme 3). In TS1 the energy of the N_α-N_β bond cleavage is compensated by the energy of new C-N bond formation between the appearing **2** NH_2^+ and benzene (Fig.4). The stabilization of **2** NH_2^+ facilitates the release of nitrogen and reduces the energy required for the **1** $H_2N_3^+$ $_{(as)}$ decomposition from 79.8 kcal/mol (pathway **B**, Scheme 2) to 14.93 kcal/mol comparing to the energy of **1** $H_2N_3^+$ $_{(as)}$ decomposition with formation of bare **2** NH_2^+. As a result, the energy required for electrophile generation in the pathway **B** is significantly higher than the energy of rate determining step in pathway **A**, hence the pathway **B** can be ruled out as less thermodynamically favorable.

It could be noted that TS1 has higher free energy in aqueous solution than in gas phase leading us to the conclusion that amination is better proceed in non-polar media rather than in polar. Indeed, Borodkin *et al* demonstrated that amination of mesitylene by NaN_3/$AlCl_3$/HCl in solvents with low polarity results in better yields of the amination products [43].
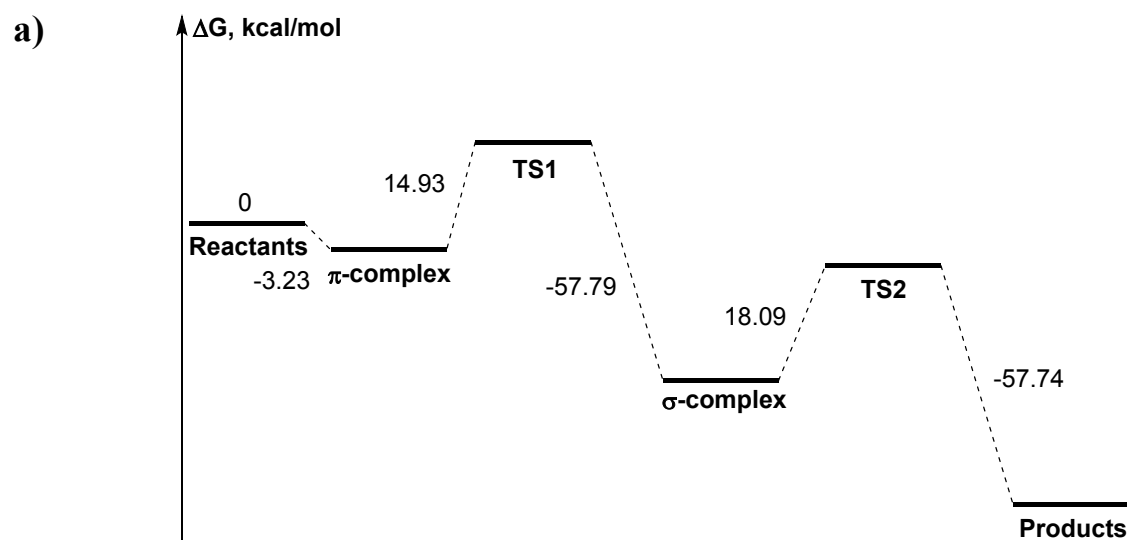
a)

b)

Scheme 3. Free energies for the stationary points on the PES in the direct amination of benzene by $H_2N_3^+{}_{(as)}$ calculated at B3LYP/aug-cc-pvdz level of theory: a) in gas phase; b) in water (CPCM solvation model).

Thus, for the first time we have clearly shown that the pathway **A** is thermodynamically favored over the pathway **B** and direct amination of arenes by hydrazoic acid proceeds via $H_2N_3^+{}_{(as)}$ as electrophile. Also, we demonstrated that direct amination refers to electrophilic aromatic substitution reactions, which rate is determined by the transition state TS1, and better proceeds in non-polar media.

In order to study the influence of the substitution in aromatic ring on the structure and energies of the stationary points on amination PES we took five monosubstituted benzenes: toluene, aniline, anisole, chlorobenzene, and nitrobenzene.

Taking *para-* isomer as an example, we may see that with an increase of ionization potential (PI) of the corresponding substituted benzene the distance between the *para*-carbon (C4) and N_α in π-complex increases. The shorter C4-N_α distance in π-complexes of benzenes with electron-donating substituents indicates stronger interaction and a more significant charge transfer between $H_2N_3^+$ $_{(as)}$ and a substrate. This further facilitates the formation of TS1 since less structural changes, and as a result, less energy is required (Table 5). It should be also noted that positional selectivity in amination already occurs in π-complexes. For example, *para*-oriented π-complexes give *para*-oriented TS1 (Fig.5). Moreover, the formation of *para*-oriented π-complexes is thermodynamically favoured over *ortho-* and *meta-* (Table 6). The exception is nitrobenzene, where no specific carbon coordination is observed in π-complex.

Table 5. *Para*-carbon and N_α distances in π-complexes (d_π), TS1 (d_{TS1}) and σ-complexes (d_σ) and differences in free energies between TS1 and π-complexes ($\Delta G_{TS1-\pi}$) and σ-complexes and TS1 ($\Delta G_{\sigma-TS1}$) for *para*-substituted anilines.

PhX; X=	PI [49], eV	d_π, Å	d_{TS1}, Å	d_σ, Å	$\Delta d_{TS1-\pi}$, Å	$\Delta G_{TS1-\pi}$, kcal/mol	$\Delta d_{TS1-\sigma}$, Å	$\Delta G_{\sigma-TS1}$, kcal/mol
NH_2	7.7	-	2.60	1.46	-	-	1.136	-71.88
OMe	8.22	2.89	2.53	1.46	0.353	12.18	1.083	-67.60
Me	8.82	2.97	2.47	1.44	0.504	13.61	1.035	-61.81
H	9.245	3.07	2.44	1.41	0.626	14.93	1.030	-57.79
Cl	9.07	-	2.47	1.44	-	-	1.033	-58.84
NO_2	9.92	3.28[a]	2.41	1.38	0.867	14.56	1.032	-51.19

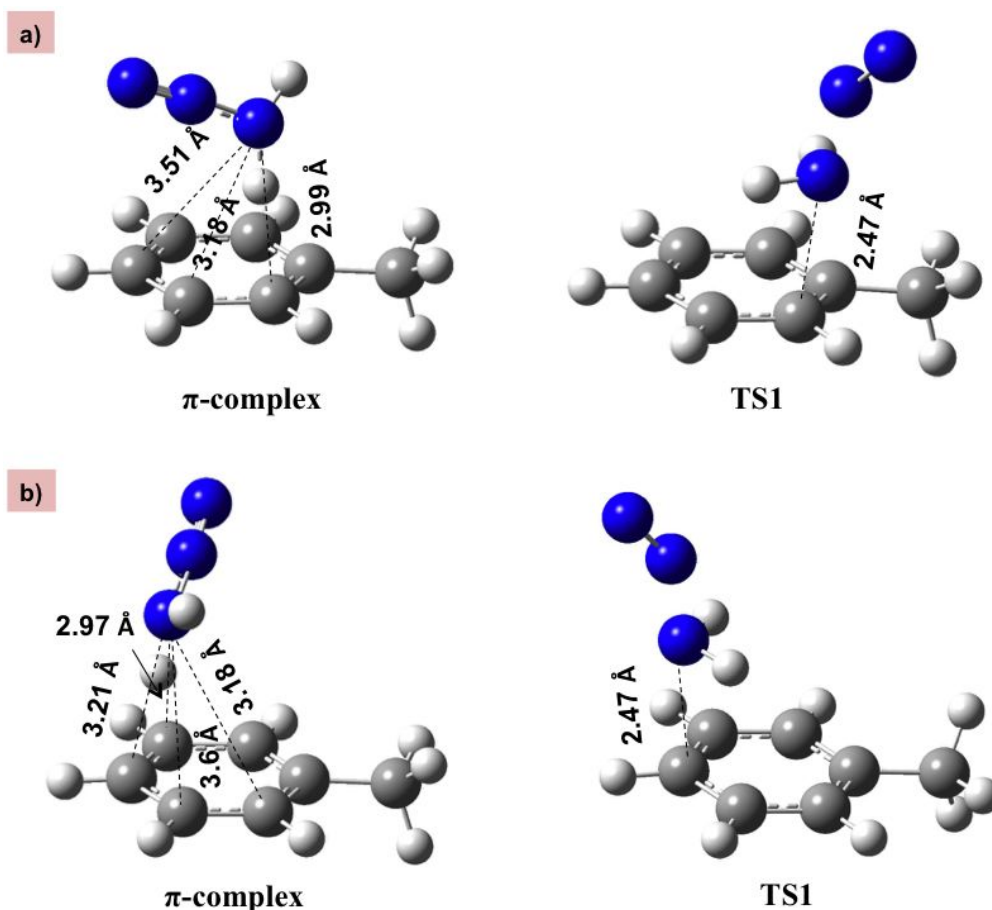[a] In case of nitrobenzene no specific carbon orientation was observed in π-complex

Fig.5. Structures of π-complexes and TS1 for *ortho*- (a) and *para*- (b) aminotoluidines formation (B3LYP/aug-cc-pVDZ).

The opposite relationship is observed between the PI and C4-N_α distance in TS1: with a decrease of PI the C4-N_α distance increases (Table 5). Indeed, the more activating substituent is the earlier rate determining TS1 is observed as the reaction rate increases [46]. Therefore, the structures and energies of rate determining TS1 of substrates with electron-donating substituents is further away from the corresponding σ-complexes. The length of the C4-N_α bond in σ-complexes decreases with an increase of PI (Table 5). Obviously, the stronger electron-withdrawing substituent stimulates the more pronounced electron donating effect of amino group resulting in a higher conjugation of appearing amino group and aromatic ring and shorter C4-N_α bond length.

It could be seen that reaction rate increases with an increase of the substrate activity: the highest rate is observed for aniline, while the lowest - for nitrobenzene (Table 6). The calculated $k_{substrate}/k_{benzene}$ ratio for toluene is 9.3/1 for *para*- and 7.1/1 for *ortho*- position (Table 6). These results are overall in agreement with the experimental data obtained by Olah et al, where $k_{substrate}/k_{benzene}$ rate for toluene was 4/1 (25 °C, $H_2N_3^+AlCl_4^-$) [16] or 3/1 (55 °C, Me_3SiN_3, TfOH) [50] depending on amination conditions. Considering the $k_{substrate}/k_{benzene}$ rate found for other arenes

(Table 5), we can conclude that both calculations and experiments show that amination has low substrate selectivity.

Table 5 shows the free energies of the stationary points on the PES for the direct amination of toluene, aniline, anisole, chlorobenzene and nitrobenzene by **1** $H_2N_3^+$ $_{(as)}$.

Toluene is activated in S_EAr and *ortho-/para-* directing. The formation of *ortho-* and *para-* oriented π-complexes between toluene and $H_2N_3^+$ $_{(as)}$ is thermodynamically favorable with *para-* position preferred over *ortho-*. For toluene the formation of TS1 is a rate determining step with the lowest activation energy for *para-* position. The thermodynamics of σ-complexes and TS2 formation shows that in both cases *para-* isomer is the most favorable and *meta-* isomer is the least favorable. However, among the products the most thermodynamically favorable is *meta-* toluidinium ion and the least thermodynamically favorable is *ortho-* toluidinium ion (Table 6).

Anisole is activated in S_EAr and *ortho-/para-* directing. The formation of *para-* oriented π-complex between anisole and $H_2N_3^+$ $_{(as)}$ requires -7.21 kcal/mol and is more thermodynamically favourable then for toluene. The energy required for TS1 formation for anisole is also reduced comparing to benzene and toluene with *para-* position preferred over *ortho-*. The same is observed in σ-complexes, whereas in TS2 and products *ortho-* isomer is thermodynamically favoured over *para-* (Table 6). We have not shown data for *meta-* oriented σ-complex and TS2 since a proton transfer with the formation of arenium ion was observed in both cases (Fig.6 a).

Chlorobenzene is deactivated in S_EAr, but *ortho-/para-* directing. The formation of π-complex between chlorobenzene and $H_2N_3^+$ $_{(as)}$ is less thermodynamically favourable then for benzene and toluene. Same as for toluene, for chlorobenzene the TS1 is a rate determining step with the lowest activation energy for *para-* position. In σ-complexes and TS2 of the chlorobenzene *para-* isomer is also the most thermodynamically favorable and *meta-* isomer is the least thermodynamically favorable.

Nitrobenzene is strongly deactivated in S_EAr and *meta-* directing. The π-complex formation between nitrobenzene and $H_2N_3^+$ $_{(as)}$ requires 7.82 kcal/mol and shows no pronounced positional selectivity: the distance between N_α and *ortho-*, *meta-* and *para-* carbon is 3.31, 3.29 and 3.28 Å, respectively. Unfortunately, we were not able to find TS1 for *meta-* isomer, but σ-complexes energies indicate *meta-* position as the most thermodynamically favorable one (Table 6). Indeed, the experiments showed, that the amination of nitrobenzene resulted in trace amount of *meta-* isomer [15].

The amination of aromatic amines is a special case. On the one hand, aniline **9** is evidently the most active aromatic substrate in the amination (Tables 5, 6). At the same time, there are no successful experimental results on its amination to date. The calculations predict that aniline **9** is *ortho-/para-* directing. We were able to find only *ortho-* oriented π-complex for aniline. *Meta-*

oriented π-complex during optimization converged to *para-*. In *para-* oriented π-complex a proton transfer with the formation of arenium ion was observed (Fig.6 b).
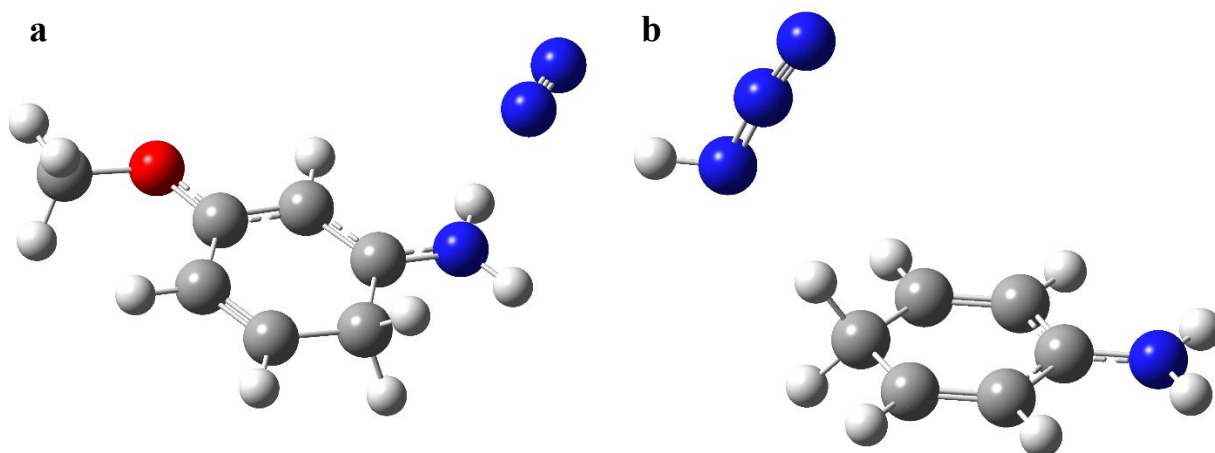
a   **b**

Fig.6. Examples of proton transfer with the formation of arenium ion: a) *meta-* oriented σ-complex of aminoanisole; b) *para-* oriented π-complex of aniline and aminodiazonium ion

The calculations show that the formation of found π-complex should proceed easily and is followed by TS1 with the lowest activation energies among the studied compounds. The *para-* position is thermodynamically favored in TS1, TS2 and products, whereas in σ-complexes the *ortho-* isomer is preferable (Table 6). Thus, the amination of aniline **9** is thermodynamically possible, however, it has not been reported experimentally. It could be explained by the different reasons. On the one hand, aniline **9** is obviously a stronger base then $H_2N_3^+$ $_{(as)}$, thus it would replace it from its salt leading to a decrease in electrophile concentration. On the other hand, in the strong acidic media there is an equilibrium between aniline **9** and anilinium ion **10** (Scheme 4). The latter is deactivated in S_EAr reactions due to the electron-withdrawing effect of NH_3^+. To identify the actual reason of aniline sluggishness in direct amination, we aminated aniline **9** and, for the first time, 1-aminonaphtalene **13** in the same conditions using NaN_3 in CF_3SO_3H.
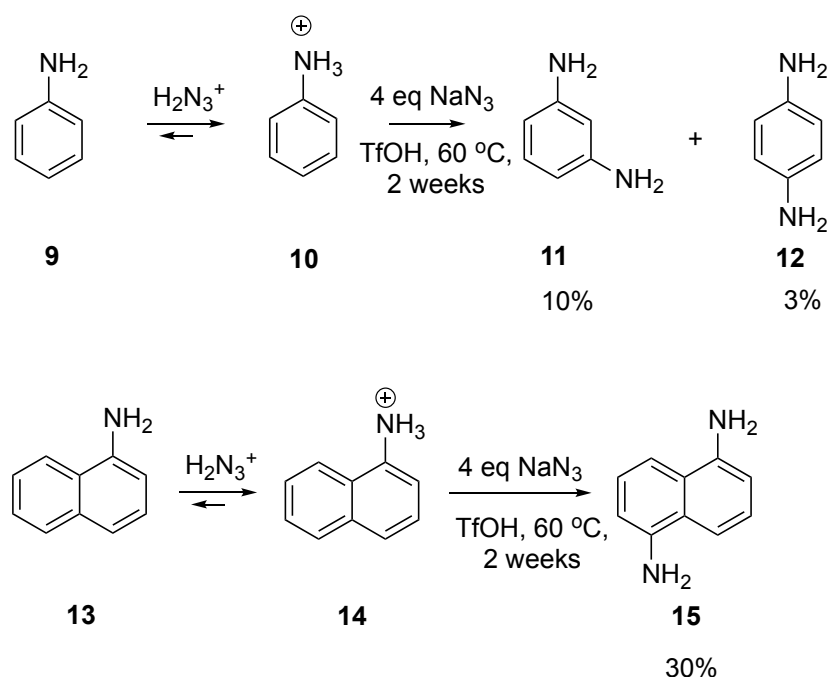
Scheme 4. Direct amination of aniline and 1-aminonaphtalene by NaN$_3$/TfOH

As a result of aniline **9** direct amination, we have obtained the reaction mixture containing aniline **9** (87%), *meta*- phenylene diamine **11** (10%) and *para*- phenylene diamine **12** (3%) according to the GC and GC-MS (Fig. 4S) data (Scheme 4). Positional selectivity for phenylene diamines was identified by comparing their retention times and R_f to pure compounds. The observed positional selectivity indicates that the major process is amination of anilinium ion. The 1-aminonaphtalene **13** amination in the same conditions resulted in 1,5-diaminonaphtalene **15** as a major product with 30% yield (Scheme 4). It is known that naphthalenes with electron-withdrawing group in 1 position undergo electrophilic substitution in 5 position. For example, electrophilic bromination of 1-nitronaphtalene yielded in 30% of 1-bromo-5-nitronaphtalene [51]. At the time, nitration of 1-aminonaphtalene in non-acidic conditions led in a mixture of 1-amino-2-nitronaphtalene and 1-amino-4-nitronaphtalene in a ratio 22:71% [52]. Therefore, our data indicate that product **15** is obtained as a result of naphthalene-1-aminium **14** amination. Thus, even if the H$_2$N$_3^+$ $_{(as)}$ is partially deactivated due to the proton exchange with anilines as the bases, the remaining amount of electrophile is still able to aminate anilinium ion.

Table 6. Free energies difference from reactants and rate constant ratios for the direct amination of aniline, anisole, toluene, benzene, chlorobenzene and nitrobenzene by **1** H$_2$N$_3^+$ $_{(as)}$.

PhX; X=	NH$_2$ position	ΔG difference from reactants, kcal/mol					$k_{subst}/k_{benzene}$
		π-complex	**TS1**	**σ-complex**	**TS2**	**Products**	

NH₂	*ortho-*	-9.38	2.60	-73.90	-35.54	-90.45	147
	meta-	-ᵃ	-ᵃ	-ᵇ	-41.12	-91.53	-
	para-	-ᵇ	-0.13	-72.01	-41.55	-91.75	1·10⁵
OMe	*ortho-*	-ᵇ	6.20	-61.37	-91.97	-36.80	13
	meta-	-ᵃ	-ᵃ	-ᵇ	-ᵇ	-35.77	-
	para-	-7.21	4.98	-62.63	-83.06	-36.16	100
Me	*ortho-*	-4.34	9.42	-51.96	-31.15	-86.71	7.1
	meta-	-ᵃ	**9.65**	-49.21	-30.70	-87.59	-
	para-	-5.25	8.36	-53.46	-32.47	-86.78	9.3
H	-	**-3.23**	**11.70**	**-33.24**	**-28.01**	**-85.75**	-
Cl	*ortho-*	-0.31	14.04	-43.73	-24.55	-83.31	2.7
	meta-	0.65	-ᵃ	-40.41	-22.78	-80.92	-
	para-	-ᶜ	13.63	-45.21	-25.00	-81.21	-
NO₂	*ortho-*		18.03	-28.66	-14.82	-80.91	5·10⁻³
	meta-	7.82	-ᵈ	-31.25	-14.52	-74.92	-
	para-		22.39	-28.80	-14.27	-74.33	3·10⁻⁶

ᵃ During optimization *meta-* position converged to *para-*

ᵇ Proton transfer was observed

ᶜ We were not able to find a π-complex

ᵈ We were not able to find TS1

Direct amination among the S_EAr reactions

In attempt to compare the direct amination with the other S_EAr reactions we calculated the rate constants for the amination of studied compounds using Eyring–Polanyi equation (eq 10). The free energies of TS1 formation were taken as activation free energies. The rate constants were then correlated with the σ_p and σ_p^+ values of the corresponding substituents [53] (-NH₂, -OMe, -Me, -H, -Cl, -NO₂). The plot showed good correlation between lg $k_{substrate}/k_{benzene}$ and σ_p ($R^2 = 0.997$, $\rho = -7.2$) and weaker correlation between lg $k_{substrate}/k_{benzene}$ and σ_p^+ ($R^2 = 0.899$, $\rho = -4.9$). In contrast, if free energies of σ-complex formation were used for the rate constants calculation the correlation was much better with σ_p^+ ($R^2 = 0.988$, $\rho = -8.5$) than with σ_p ($R^2 = 0.908$, $\rho = -10.7$). The similar results were observed in [46], where authors correlated computed activation free energies and free energies of σ-complex formation with σ_m/σ_p and σ_m^+/σ_p^+ for nitration. For amination as well as for

nitration the correlations are consistent with early rate-determining TS when the positive charge is located on electrophile and bond between nitrogen and aromatic carbon has not been formed. In contrast, in σ-complex there is a resonance interaction between the substituent and the positive charge in substitution site [46], which explains better correlation with σ_p^+. As authors of [46] we have also observed that the substituent effect on the free energy for σ-complex is more pronounced compared to TS1 (Table 6). It is interesting though that there is a strong correlation between Gibbs free energies of TS1 and σ-complexes ($R^2 = 1$, data for *para-* position) that might indicate that we have found correct TS on PES.

Table 7. The reaction constants for S_EAr reactions

| Reaction	ρ
Bromination (CH$_3$COOH) [53]	-13.1
Chlorination (CH$_3$COOH+H$_2$O) [53]	-13.0
Acylation (CH$_3$COCl, AlCl$_3$, C$_2$H$_2$Cl$_2$) [53]	-8.6
Amination (HN$_3$)	*-4.9 [a] / -8.5 [b]*
Nitration (H$_2$SO$_4$+HNO$_3$) [53]	-6.4
Amination (PhXN$_3$, AlCl$_3$) [54]	-6.0
Amination (PhXN$_3$, CF$_3$COOH, CF$_3$SO$_3$H) [55]	-4.5

[a] found using the free energies of TS1 formation for the rate constants calculation

[b] found using the free energies of σ-complex formation for the rate constants calculation

The predicted ρ values and observed similarities allowed us to put amination of arenes by H$_2$N$_3^+$ somewhere close to nitration (Table 7). As we stated above, amination is characterized by an earlier transition state than halogenations since TS1 in amination shows more similarity to the π-complex, whereas TS in halogenations is more similar to the σ-complex [47,48]. Nitration was also shown to have an earlier transition state than halogenations [46]. It is quite complicated to compare nitration and amination in terms of TS location. On the other hand, it is well known that nitration of aniline gives a mixture of *para-* and *meta-* isomers in a ratio of 51% to 47% with 95% yield, while amination of aniline results in only traces of *meta-* (10%) and *para-* (3%) phenylenediamines. In both cases, aniline forms a conjugated acid due to strong acidic conditions and becomes deactivated. However, it still undergoes nitration in rigorous conditions, while more sluggish to amination. We may observe the same situation for nitration and amination of nitrobenzene. From this point we may say that amination is quite similar to a Friedel-Crafts alkylation and acylation, which also almost do not proceed with strongly deactivated substrates. Thus, direct amination refers to electrophilic substitution reactions with an early transition state.

Future of direct amination

Strong acidic conditions required for amination of arenes by HN_3 significantly reduce the number of substrates suitable for amination. To overcome this problem, the derivatives of HN_3 such as arylazides can be used. For comparison, we found the thermodynamic characteristics of **18** $PhNH^+$ formation from **16** (**17**) $PhHN_3^+$ (Scheme 5).
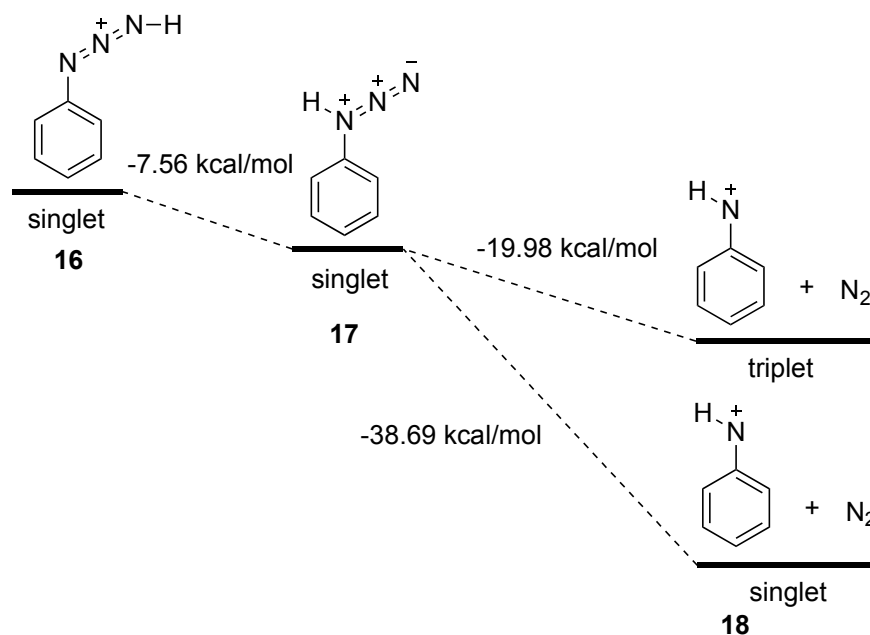
Scheme 5. Thermodynamic characteristics of $PhNH^+$ formation from $PhHN_3^+$ in gas phase (B3LYP/aug-cc-pVDZ).

The conjugation between of NH^+ and aromatic ring stabilizes the appearing nitrenium ion **18** and significantly decreases the energy of nitrogen cleavage. It makes the process of **18** $PhNH^+$ formation thermodynamically favourable that, in turn, makes **16** (**17**) $PhHN_3^+$ totally different from **1** $H_2N_3^+$ (as). The calculation results are supported by the fact that arylazides react with benzene giving diphenylamines in the presence of CF_3COOH [55], i.e. in much less acidic conditions than required for direct amination of arenes with HN_3. However, the mechanism of direct amination of arenes by **16** (**17**) $PhHN_3^+$ and its derivatives require special investigation.

Apparently, the use of organic azides for amination might be promising as reaction would proceed in milder conditions.

Conclusions

Overall, for the first time, using quantum chemical calculations we have shown that direct amination of arenes by hydrazoic acid follows the classical S_EAr mechanism with aminodiazonium cation $H_2N_3^+$ (as) as electrophile. The $H_2N_3^+$ (as) has been found to be a very special diazonium cation with high dediazotization energy. Using method for tracing of the molecular orbitals we have shown that the peculiarity of the $H_2N_3^+$ (as) electronic structure is that the N_2 HOMO energy (-0.438559 Ha) is higher than the NH_2^+ LUMO energy (-0.610093 Ha), which leads to a very slow separation of these orbitals during the nitrogen elimination. The located stationary points allowed us to define direct amination as S_EAr reaction, which rate is determined by the transition state between π- and σ-complexes. The positional selectivity in amination already occurs in π-complexes making their formation an important step along the reaction pathway. The structural similarity between the transition state and π-complex shows that direct amination has an early transition state. The comparison of amination and other S_EAr reactions in terms of transition state location allowed us to place it somewhere in-between nitration and halogenations closer to nitration and Friedel-Crafts alkylation/acylation. We also predicted that amination by HN_3 better proceeds in non-polar media rather than in polar. For the first time we have studied the acidity of hydrazoic acid and $H_2N_3^+$ and calculated their pK_a. We have shown that an acid stronger than $H_2N_3^+$ (as) with pK_a lower than approximately -5.32 is required for the direct amination with HN_3. This explains why amination took place only in the presence of superacids or Lewis acids. These results open a prospect for identification of the new aminating agents working in milder conditions. We also argue that using organic azides, such as phenylazide, instead of HN_3 for the amination of arenes, can be energetically more beneficial and safer.

Experimental section

General remarks

All the reagents were ACS grade and used without further purification. 1H NMR and 13C NMR spectra were recorded using Bruker AVANCE III HD spectrometer at 400 MHz and 100.5 MHz, respectively. IR spectra were recorded in ATR mode (ZnSe crystal) with Agilent Cary 630 FTIR (Agilent Technologies, USA). GC/MS analysis was performed using Agilent 7890/5975C system. Melting points (uncorrected) were measured using melting point system MP50 (Mettler, Toledo).

Amination of aniline (9)

Sodium azide (8 mmol, 520 mg) was added by four portions every hour to a solution of aniline (**9**) (2 mmol, 0,182 ml) in trifluoromethanesulfonic acid (2 ml). The reaction mixture was heated at 60 ^{o}C for two weeks with stirring. The progress of the reaction was monitored by the consumption of the starting aniline using TLC (eluent – ethylacetate/hexane=2/1. The analysis of the reaction mixture was performed using GC, GC/MS (Fig. 4S), and TLC and showed three compounds: aniline, 1,3 - benzene diamine and 1,4 - benzene diamine in a ratio of 87:10:3%. The identities of the products were confirmed by comparing their retention times and R_f to pure commercially available compounds. The following retention times and R_f were found for pure benzene diamine isomers: 1,2 - benzene diamine (T retention 7.913 min, R_f = 0.39), 1,3 - benzene diamine (T retention 8.783 min, R_f = 0.19), 1,4 - benzene diamine (T retention 8.443 min, R_f = 0.27).

Aniline (9): GC-MS (EI), T retention 4.955 min (for pure aniline T retention 4.963 min**)**: m/z (%) = 93 (100) [M$^+$], 92 (12.5), 66 (32.5), 63 (5), 52 (4.5). TLC (eluent – ethylacetate/hexane=2/1): R_f = 0.63 (for pure aniline R_f = 0.63**).**

1,4 - Benzene diamine (11): GC-MS (EI), T retention 8.577 min (for pure 1,4 - Benzene diamine T retention 8.443 min**)**: m/z (%) = 108 (100) [M$^+$], 107 (21.3), 80 (36.8), 53 (13.6). TLC (eluent – ethylacetate/hexane=2/1): R_f = 0.27 (for pure 1,4 - Benzene diamine R_f = 0.27**).**

1,3 - Benzene diamine (12): GC-MS (EI), T retention 8.807 min (for pure 1,3 - Benzene diamine T retention 8.783 min): m/z (%) = 108 (100) [M$^+$], 107 (10.6), 91 (5.6), 80 (43.4). TLC (eluent – ethylacetate/hexane=2/1): R_f = 0.19 (for pure 1,3 - Benzene diamine R_f = 0.19).

Amination of 1-aminonaphtalene (13)

Sodium azide (8 mmol, 520 mg) was added by four portions every hour to a solution of 1-aminonaphtalene (**13**) (2 mmol, 286 mg) in trifluoromethanesulfonic acid (2 ml). The reaction mixture was heated at 60 ^{o}C for two weeks with stirring. The progress of the reaction was monitored by the consumption of the starting 1-aminonaphtalene (**13**) using TLC (eluent - ethylacetate/hexane=2/1). The reaction mixture was poured into water (50 ml), neutralized by NaOH until pH 7-8 and extracted with ethylacetate. Organic layer was dried over Na$_2$SO$_4$ and the solvent was removed under reduced pressure. Total yield was 354 mg. Purification by column chromatography using ethylacetate over silica gel gave two major fractions: first fraction (1-aminonaphtalene (**13**)), yield 217 mg (61%), second fraction (1,5-diaminonaphtalene (**15**)), yield 106 mg (30%).

1-aminonaphtalene (13): Pink solid; yield 217 mg (61%). m.p. 50-51 °C (lit. m.p. 48-50 °C [56]). ^{1}H NMR (400 MHz, DMSO-d_6): δ = 8.07 (d, J= 8 Hz, 1H, 8-CH$_{Ar}$), 7.73(d, J= 8 Hz, 1H, 5-CH$_{Ar}$), 7.38 (m, 2H, 6,7-CH$_{Ar}$), 7.21 (m, 1H, 3-CH$_{Ar}$), 7.08 (d, J= 8 Hz, 1H, 4-CH$_{Ar}$), 6.69 (d, J= 8 Hz, 1H, 2-CH$_{Ar}$), 5.72 (s, NH$_2$) ppm. ^{13}C NMR (100.5 MHz, DMSO-d_6): δ = 145.15, 134.65, 128.28, 127.21, 125.95, 124.10, 123.10, 122.80, 115.85, 107.90 ppm. IR: 3411 cm^{-1}, 3340 cm^{-1}, 3230 cm^{-1}. GC-MS (EI), T retention 11.061 min: m/z (%) = 143 (100) [M$^+$], 116 (18), 115 (43), 89 (5), 71.5 (7), 63 (5).

1,5-diaminonaphtalene (15): Brown solid; yield 106 mg (30%). m.p. 187 °C (lit. m.p. 188 °C [57]). ^{1}H NMR (400 MHz, DMSO-d_6): δ = 7.22(d, J= 8 Hz, 2H, 4,8-CH$_{Ar}$), 7.07 (m, 2H, 3,7-CH$_{Ar}$), 6.61 (d, J= 8 Hz, 2H, 2,6-CH$_{Ar}$), 5.44 (s, NH$_2$) ppm. ^{13}C NMR (100.5 MHz, DMSO-d_6): δ = 144.97, 124.82, 124.22, 110.47, 107.90 ppm. IR: 3424 cm^{-1}, 3413 cm^{-1}, 3320 cm^{-1}, 3226 cm^{-1}. GC-MS (EI), T retention 13.757 min: m/z (%) = 158 (100) [M$^+$], 141 (4), 131 (6), 130 (27), 118 (5), 103 (9), 79 (9), 65 (4).

Caution! *Volatile, highly toxic, and explosive HN$_3$ can occasionally evolve and these operations need to be conducted in a well-ventilated exhaust hood.*

Supporting Information

Geometry of H$_3$O$^+$(H$_2$O)$_3$, cluster, the energies of individual MO over increasing N$_\alpha$-N$_\beta$ distance during N$_2$ elimination from, the energy diagram of the formation of 1 H$_2$N$_3^+$ $_{(as)}$ from 2 NH$_2^+$ and N$_2$, table of the structural parameters of [NH$_2$ + N$_2$]$^+$, table of thermodynamics of various pathways of H$_2$N$_3^+$ $_{(as)}$ decomposition, the videos of all MO transformations, NMR, IR and GC-MS spectra of the synthesized compounds.

Acknowledgments

References

(1)   Bräse, S. *Amino Group Chemistry: From Synthesis to the Life Sciences. Edited by Alfredo*

Ricci.; 2008; Vol. 9.

(2)   Tafesh, A. M.; Weiguny, J. A Review of the Selective Catalytic Reduction of Aromatic
        Nitro Compounds into Aromatic Amines, Isocyanates, Carbamates, and Ureas Using CO
        †. *Chem. Rev.* **1996**, *96* (6), 2035–2052.

(3)   Downing, R. S.; Kunkeler, P. J.; van Bekkum, H. Catalytic Syntheses of Aromatic
        Amines. *Catal. Today* **1997**, *37* (2), 121–136.

(4)   Aubin, Y.; Fischmeister, C.; Thomas, C. M.; Renaud, J.-L. Direct Amination of Aryl
        Halides with Ammonia. *Chem. Soc. Rev.* **2010**, *39* (11), 4130.

(5)   Coeffard, V.; Moreau, X.; Thomassigny, C.; Greck, C. Transition-Metal-Free Amination
        of Aryl Boronic Acids and Their Derivatives. *Angew. Chemie Int. Ed.* **2013**, *52* (22),
        5684–5686.

(6)   Li, B.; Sortais, J.-B.; Darcel, C. Amine Synthesis via Transition Metal Homogeneous
        Catalysed Hydrosilylation. *RSC Adv.* **2016**, *6* (62), 57603–57625.

(7)   Yazaki, R. Nucleophilic Amination Strategy for Catalytic Synthesis of α-Amino Carbonyl
        Compounds. *J. Synth. Org. Chem. Japan* **2016**, *74* (7), 732–733.

(8)   Grange, R.; Clizbe, E.; Evans, P. Recent Developments in Asymmetric Allylic Amination
        Reactions. *Synthesis (Stuttg).* **2016**, *48* (18), 2911–2968.

(9)   Becker, J.; Hölderich, W. F. Amination of Benzene in the Presence of Ammonia Using a
        Group VIII Metal Supported on a Carrier as Catalyst. *Catal. Letters* **1998**, *54* (3), 125–
        128.

(10)   Hagemeyer, A.; Borade, R.; Desrosiers, P.; Guan, S.; Lowe, D. M.; Poojary, D. M.;
        Turner, H.; Weinberg, H.; Zhou, X.; Armbrust, R.; et al. Application of Combinatorial
        Catalysis for the Direct Amination of Benzene to Aniline. *Appl. Catal. A Gen.* **2002**, *227*
        (1–2), 43–61.

(11)   Kovacic, P.; Bennett, R. P.; Foote, J. L. Aromatic Amination with Hydroxylammonium
        Salts. Reactivity and Directive Effects. *J. Am. Chem. Soc.* **1962**, *84* (5), 759–763.

(12)   Kovacic, P.; Bennett, R. P. Aromatic Amination with Hydroxylamine-O-Sulfonic Acid 1.
        J. Am. Chem. Soc. **1961**, *83* (1), 221–224.

(13)   Kovacic, P.; Foote, J. L. Aromatic Amination with Alkylhydroxylamines 1,2. *J. Am.
        Chem. Soc.* **1961**, *83* (3), 743–747.

(14)   Takeuchi, H.; Adachi, T.; Nishiguchi, H.; Itou, K.; Koyama, K. Direct Aromatic
        Amination by Azides: Reactions of Hydrazoic Acid and Butyl Azides with Aromatic
        Compounds in the Presence of Both Trifluoromethanesulfonic Acid and Trifluoroacetic
        Acid. *J. Chem. Soc. Perkin Trans. 1* **1993**, No. 7, 867.

(15)   Prakash, G. K. S.; Gurung, L.; Marinez, E. R.; Mathew, T.; Olah, G. A. Electrophilic

Amination of Aromatics with Sodium Azide in BF3–H2O. *Tetrahedron Lett.* **2016**, *57* (3), 288–291.

(16)   Olah, G. A. Onium Ions. 26. Aminodiazonium Ions: Preparation, Proton, Carbon-13, and Nitrogen-15 NMR Structural Studies, and Electrophilic Amination of Aromatics. *J. Am. Chem. Soc.* **1983**, *105* (17), 5657–5660.

(17)   Hoop, G.M.; Tedder, J. M. The Direct Amination of Mesitylene by Hydraxoic Acid in Concentrated Sulphuric Acid. *J. Chem. Soc.* **1961**, 4685–4687.

(18)   Aksenov, A. V.; Lyakhovnenko, A. S.; Kugutov, M. M. New Method for the Direct Electrophilic Amination of Aromatic Compounds and Its Use in the Annelation of the Pyrimidine Ring. *Chem. Heterocycl. Compd.* **2011**, *46* (10), 1262–1265.

(19)   Borodkin, G. I.; Shubin, V. G. Nitrenium Ions and Problem of Direct Electrophilic Amination of Aromatic Compounds. *Russ. J. Org. Chem.* **2005**, *41* (4), 473–504.

(20)   Raap, R. Amination of Tetrazoles with Hydroxylamine- O -Sulfonic Acid: 1- and 2-Aminotetrazoles. *Can. J. Chem.* **1969**, *47* (19), 3677–3681.

(21)   Garman, K.; Olewnik, E.; Czerwinski, W. Synthesis of Alkylcarbazole Aminoderivatives. *Heteroat. Chem.* **2012**, *23* (1), 1–4.

(22)   Aksenov, A. V.; Lyakhovnenko, A. S.; Karaivanov, N. C.; Levina, I. I. Synthesis and Special Features of the Structure of 6(7)-Aminoperimidine Derivatives. *Chem. Heterocycl. Compd.* **2010**, *46* (4), 468–472.

(23)   Borodkin, G. I.; Elanov, I. R.; Shubin, V. G. Electrophilic Amination of Methylbenzenes with Sodium Azide in Trifluoromethanesulfonic Acid. *Russ. J. Org. Chem.* **2009**, *45* (6), 934–935.

(24)   Frisch, M. J., Trucks, G. W., Schlegel, H. B., Scuseria, G. E., Robb, M. A., Cheeseman, J. R., Scalmani, G., Barone, V., Mennucci, B., Petersson, G. A., Nakatsuji, H., Caricato, M., Li, X., Hratchian, H. P., Izmaylov, A. F., Bloino, J., Zheng, G., Sonnenb, D. J. Gaussian 09. Gaussian, Inc., Wallingford CT 2009.

(25)   Neese, F. The ORCA Program System. *Wiley Interdiscip. Rev. Comput. Mol. Sci.* **2012**, *2* (1), 73–78.

(26)   Becke, A. D. Density-Functional Exchange-Energy Approximation with Correct Asymptotic Behavior. *Phys. Rev. A* **1988**, *38* (6), 3098–3100.

(27)   Lee, C.; Yang, W.; Parr, R. G. Development of the Colle-Salvetti Correlation-Energy Formula into a Functional of the Electron Density. *Phys. Rev. B* **1988**, *37* (2), 785–789.

(28)   Peverati, R.; Truhlar, D. G. Improving the Accuracy of Hybrid Meta-GGA Density Functionals by Range Separation. *J. Phys. Chem. Lett.* **2011**, *2* (21), 2810–2817.

(29)   Binkley, J. S.; Pople, J. A. Møller-Plesset Theory for Atomic Ground State Energies. *Int.*

J. Quantum Chem. **1975**, *9* (2), 229–236.

(30)   Kendall, R. A.; Dunning, T. H.; Harrison, R. J. Electron Affinities of the First-row Atoms
Revisited. Systematic Basis Sets and Wave Functions. *J. Chem. Phys.* **1992**, *96* (9), 6796–
6806.

(31)   Dunning, T. H. Gaussian Basis Sets for Use in Correlated Molecular Calculations. I. The
Atoms Boron through Neon and Hydrogen. *J. Chem. Phys.* **1989**, *90* (2), 1007–1023.

(32)   Hehre, W. J., Radom, L., Schleyer, P. v. R., Pople, J. A. *Ab Initio Molecular Orbital
Theory*; John Wiley, New York, 1986.

(33)   Pliego, J. R.; Riveros, J. M. Theoretical Calculation of p K a Using the
Cluster−Continuum Model. *J. Phys. Chem. A* **2002**, *106* (32), 7434–7439.

(34)   Pliego, J. R.; Riveros, J. M. The Cluster−Continuum Model for the Calculation of the
Solvation Free Energy of Ionic Species. *J. Phys. Chem. A* **2001**, *105* (30), 7241–7247.

(35)   Bondarev, A. Molecular-Orbitals-Tracer, 10.5281/ZENODO.1473203. **2018**.

(36)   Evers, J.; Göbel, M.; Krumm, B.; Martin, F.; Medvedyev, S.; Oehlinger, G.; Steemann, F.
X.; Troyan, I.; Klapötke, T. M.; Eremets, M. I. Molecular Structure of Hydrazoic Acid
with Hydrogen-Bonded Tetramers in Nearly Planar Layers. *J. Am. Chem. Soc.* **2011**, *133*
(31), 12100–12105.

(37)   Christe, K. O.; Wilson, W. W.; Dixon, D. A.; Khan, S. I.; Bau, R.; Metzenthin, T.; Lu, R.
The Aminodiazonium Cation, H2N3+. *J. Am. Chem. Soc.* **1993**, *115* (5), 1836–1842.

(38)   Ford, G. P.; Herman, P. S. Energetics of the Singlet and Triplet States of Alkylnitrenium
Ions: Ab Initio Molecular Orbital Calculations. *J. Am. Chem. Soc.* **1989**, *111* (11), 3987–
3996.

(39)   Zollinger, H. Diazo Chemistry I: Aromatic and Heteroaromatic Compounds; VCH,
Weinheim, 1994; pp 221–288.

(40)   Gibson, S. T.; Greene, J. P.; Berkowitz, J. Photoionization of the Amidogen Radical. *J.
Chem. Phys.* **1985**, *83* (9), 4319–4328.

(41)   Holleman, A. F.; Wiberg, E.; Wiberg, N. *Inorganic Chemistry*; Eagleson, M., Brewer, W.,
Eds.; Academic Press, 2001.

(42)   Namazian, M.; Zakery, M.; Noorbala, M. R.; Coote, M. L. Accurate Calculation of the
PKa of Trifluoroacetic Acid Using High-Level Ab Initio Calculations. *Chem. Phys. Lett.*
2008, *451* (1–3), 163–168.

(43)   Borodkin, G. I.; Elanov, I. R.; Popov, S. A.; Pokrovskii, L. M.; Shubin, V. G.
Electrophilic Amination of Methylbenzenes with the System NaN3-AlCl3-HCl. Effects of
the Solvent, Crown Ether, and Substrate Structure. *Russ. J. Org. Chem.* **2003**, *39* (5), 672–
679.

(44) Kovacic, P.; Russell, R. L.; Bennett, R. P. Aromatic Amination with Hydrazoic Acid Catalyzed by Lewis Acids. Orientation, Activity, and Relative Rates. *J. Am. Chem. Soc.* **1964**, *86* (8), 1588–1592.

(45) Bräse, S.; Dahmen, S.; Popescu, C.; Schroen, M.; Wortmann, F.-J. The Structural Influence in the Stability of Polymer-Bound Diazonium Salts. *Chem. - A Eur. J.* **2004**, *10* (21), 5285–5296.

(46) Liljenberg, M.; Stenlid, J. H.; Brinck, T. Mechanism and Regioselectivity of Electrophilic Aromatic Nitration in Solution: The Validity of the Transition State Approach. *J. Mol. Model.* **2018**, *24* (1), 15.

(47) Filimonov, V. D.; Poleshchuk, O. K.; Krasnokutskaya, E. A.; Frenking, G. DFT Investigation of the Thermodynamics and Mechanism of Electrophilic Chlorination and Iodination of Arenes. *J. Mol. Model.* **2011**, *17* (11), 2759–2771.

(48) Liljenberg, M.; Stenlid, J. H.; Brinck, T. Theoretical Investigation into Rate-Determining Factors in Electrophilic Aromatic Halogenation. *J. Phys. Chem. A* **2018**, *122* (12), 3270–3279.

(49) Isaacs, N. S. Physical Organic Chemistry. **1968**, *1*, 877.

(50) Olah, G. A.; Ernst, T. D. Trimethylsilyl Azide/Triflic Acid, a Highly Efficient Electrophilic Aromatic Amination Reagent. *J. Org. Chem.* **1989**, *54* (5), 1203–1204.

(51) Ospina, F.; Ramirez, A.; Cano, M.; Hidalgo, W.; Schneider, B.; Otálvaro, F. Synthesis of Positional Isomeric Phenylphenalenones. *J. Org. Chem.* **2017**, *82* (7), 3873–3879.

(52) Iranpoor, N.; Firouzabadi, H.; Nowrouzi, N.; Firouzabadi, D. Highly Chemoselective Nitration of Aromatic Amines Using the Ph3P/Br2/AgNO3 System. *Tetrahedron Lett.* **2006**, *47* (38), 6879–6881.

(53) Carey, F. A.; Sundberg, R. J. *Advanced Organic Chemistry Part A: Structure and Mechanisms*; 2007.

(54) Takeuchi, H.; Maeda, M.; Mitani, M.; Koyama, K. Inter- and Intra-Molecular Aromatic N-Substitution by Arylnitrenium–Aluminium Chloride Complexes Generated from Aryl Azides in the Presence of Aluminium Chloride. *J. Chem. Soc., Perkin Trans. 1* **1987**, 57–60.

(55) Takeuchi, H.; Takano, K. Aromatic Substitution by Phenylnitrenium and Naphthylnitrenium Ions Formed from Phenyl Azide and 1-Azidonaphthalene in the Presence of Trifluoromethanesulphonic Acid. *J. Chem. Soc. Chem. Commun.* **1983**, No. 8, 447.

(56) Aksenov, A. V.; Lyakhovnenko, A. S.; Andrienko, A. V. Synthesis of 1H-1,5,7-Triazacyclopenta[c,d]Phenalenes by the Electrophilic Amination of Perimidines Using

Sodium Azide in PPA. *Chem. Heterocycl. Compd.* **2011**, *46* (10), 1266–1270.

(57)   Ayyangar, N. R.; Kalkote, U. R.; Lugade, A. G.; Nikrad, P. V.; Sharma, V. K. Partial Reduction of Dinitroarenes to Nitroanilines with Hydrazine Hydrate. *Bull. Chem. Soc. Jpn.* **1983**, *56* (10), 3159–3164.

For Table of Contents Only